Geochimica et Cosmochimica Acta 379 (2024) 23–38

Contents lists available at ScienceDirect

Geochimica et Cosmochimica Acta

journal homepage: www.elsevier.com/locate/gca

Understanding microtektite formation: Potassium isotope evidence for condensation in a vapor plume

Piers Koefoed [a,*], Luigi Folco [b,c], Gianfranco Di Vincenzo [d], Nicole X. Nie [e], Billy P. Glass [f], Mason Neuman [a], Kun Wang (王昆)[a]

[a] McDonnell Center for the Space Sciences and Department of Earth, Environmental, and Planetary Sciences, Washington University in St. Louis, St. Louis, MO 63130, USA
[b] Dipartimento di Scienze della Terra, Università di Pisa, 56126 Pisa, Italy
[c] CISUP, Centro per l'Integrazione della Strumentazione dell'Università di Pisa, 56126 Pisa, Italy
[d] Istituto di Geoscienze e Georisorse – CNR, via Moruzzi 1, 56124 Pisa, Italy
[e] Department of Earth, Atmospheric and Planetary Sciences, Massachusetts Institute of Technology, Cambridge, MA 02139, USA
[f] Department of Earth Sciences, The University of Delaware, Newark, DE 19716, USA

ARTICLE INFO

Associate editor: Tomas Magna

Keywords:
K isotopes
Tektite
Microtektite
Condensation
Evaporation
Impact plume

ABSTRACT

Tektite and microtektite formation have important implications on our understanding of impacts both on Earth, the Moon and on other bodies within our solar system. Here, we investigate the formation mechanisms of microtektites by analysing the K isotope systematics and elemental compositions of forty-four Australasian microtektites from various distances from the proposed impact location. Based on the K isotope and concentration data, the microtektites analyzed here are split into two groups, the "ODP group" and the "MB group". The ODP group were recovered from the Ocean Drilling Project (ODP) sediment cores and consist of microtektites which landed closer to the proposed impact site (~1220–1240 km) and show limited δ^{41}K variation (–1.06 ‰ to −0.21 ‰) and higher K concentrations (2.48 wt% to 3.66 wt% K_2O). In contrast, the MB group were mostly collected from the surface of Miller Butte (MB) in Antarctica and represent microtektites which landed significantly further from the proposed impact site (~4100–10800 km) and contain large δ^{41}K variations (−4.04 ‰ to 0.57 ‰) and low K concentrations (0.49 wt% to 1.45 wt% K_2O). For the microtektites studied here, the overall correlation observed is consistent with condensation whereby a greater extent of K depletion correlates with lighter K isotope compositions. This simple condensation model is in contrast to previous studies which find evidence for complex evolution involving evaporation, condensation, and mixing. For the ODP group microtektites, the isotopic and elemental data suggest condensation from an upper continental crust (UCC) starting composition. Conversely, for the MB group a UCC starting composition is not compatible, as even the most K-rich MB group microtektites are significantly depleted in K and display δ^{41}K values much higher than the UCC. These observations can be explained by a vapor plume with a progressively evolving K isotope composition, with the earliest K condensates depleting and fractionating K within the plume, thus altering the starting K compositions for the later K condensates. From this data we calculate a cooling rate of up to 2,600 K/hour for the ODP group and up to 20,000 K/hour for the MB group, which are comparable to the cooling rates measured for tektites and considerably faster than those theoretically calculated or experimentally determined for chondrules. Overall, when assessed within the context of previous studies, microtektite formation appears very complex with evidence for different volatilization processes to different degrees observed within different microtektites. As such, while condensation appears dominant for K within the Australasian microtektites studied here, more work is needed to fully untangle the processes involved in microtektite formation.

* Corresponding author at: McDonnell Center for the Space Sciences, Washington University in St. Louis, St. Louis, MO 63130, USA.
E-mail address: piers.koefoed@wustl.edu (P. Koefoed).

https://doi.org/10.1016/j.gca.2024.06.015
Received 19 December 2023; Accepted 18 June 2024
Available online 2 July 2024

1. Introduction

Tektites are natural siliceous glass ejecta formed by the rapid heating and quenching of terrestrial rocks by the hyper-velocity impact of an extraterrestrial object into Earth's crust (Glass, 1990; Koeberl, 1986, 1992). The size of tektites can vary significantly, with the largest reaching tens of cm in diameter and the smallest being sub millimeter. Of these size groups, tektites with a diameter of less than 1 mm are classified as microtektites. While the study of tektites and microtektites has advanced significantly over the last few decades, many aspects surrounding their formation are still not well understood. In regard to microtektites, the exact role evaporation and condensation played in their formation, and thus the implications this would have on their formation process, has not yet been conclusively resolved. As such, further study into the formation of microtektites is necessary. Additionally, microtektites provide an ideal terrestrial analog for hypervelocity impacts which occurred in the early Solar System, so gaining a greater understanding of microtektite formation could potentially have significant implications for understanding our Solar System.

Both tektites and microtektites are found within several distinct large areas across the surface of the Earth known as strewn fields. Currently, four distinct strewn fields are confirmed: the North American, Central European, Ivory Coast, and Australasia strewn fields (see, e.g., Barnes, 1963; Gentner et al., 1967; Glass, 1990; Koeberl, 1986; O'Keefe, 1976; Simonson and Glass, 2004; Zähringer and Gentner, 1963). A possible fitfh field is also present in Beleze, however there is still some debate surrounding this (Koeberl et al., 2022; Rochette et al., 2021). Of these strewn fields, the Australasian strewn field is the youngest with an age of ~800 ka (e.g., Di Vincenzo et al., 2021; Folco et al., 2008; Jourdan et al., 2019; Schwarz et al., 2016; Zähringer and Gentner, 1963). The Australasian strewn field is also the largest, covering ~15 % of the Earth's surface, with the furthest microtektites having traveled ~12,000 km (Folco et al., 2016; Folco et al., 2008; Glass and Simonson, 2013; Soens et al., 2021; Van Ginneken et al., 2018). Microtektites from the Australasian strewn field have been found over a wide variety of locations, including ocean drilling cores in the western Pacific and Indian Ocean and on land in Antarctica (e.g., Folco et al., 2009; Folco et al., 2008; Glass, 1967; Glass, 1978; Glass and Koeberl, 2006; Van Ginneken et al., 2018). Yet, even with its large size and young age, the Australasian strewn field is the only currently known strewn field without a confirmed identified impact site (e.g., Glass and Simonson, 2013). Nevertheless, based on petrographic and geochemical data along with distribution and abundance patterns, the impact site has been suggested to be in the Southeast Asia region, possibly somewhere in Indochina (Burns and Glass, 1989; Folco et al., 2010; Glass and Pizzuto, 1994; Hartung, 1990; Hartung and Koeberl, 1994; Lee and Wei, 2000; Ma et al., 2004; Rochette et al., 2018; Sieh et al., 2020; Mizera et al., 2016; Stauffer, 1978; Wasson, 1991; Whymark, 2021).

The extreme distance traveled by some of the Australasian microtektites indicates that they likely underwent more severe temperature/time regimes compared to microtektites which traveled a shorter distance from their source (e.g., Folco et al., 2010a,b). Indeed, within the microtektites from the Australasian strewn field, there is an observed depletion in the moderately volatile elements (MVE) Na and K which correlates with distance from the suggested source crater region (Folco et al., 2010a). While the mechanism of this depletion is still not completely understood, evaporation of a melt is generally the favored dominant process, due mostly to the finding of partially melted relicts of precursor rock found within some Australasian microtektites (Folco et al., 2010a; Folco et al., 2010b). Many Australasian microtektites also contain vesicles, melted quartz grains (i.e., lechatelierite), and exhibit schlieren, all of which are consistent with microtektites forming as melt droplets, rather than as a condensate (Folco et al., 2010b; Glass, 1990; Glass and Koeberl, 2006). Nevertheless, some evidence for condensation processes along with evaporation have also been observed in in some Australasian microtektites using stable isotope systematics of K (Herzog et al., 2008). Additionally, a recent study of Fe isotope compositions in Australasian microtektites indicates a convoluted process involving evaporation, condensation, and mixing (Chernonozhkin et al., 2021). For tektites, which have been the subject of extensive isotopic studies compared to microtektites, the evidence for evaporative loss of MVE being the dominant process is greater, with Cu, Zn, Sn, and Pb showing trends of heavier isotopes with increasing element depletion (Ackerman et al., 2020; Creech et al., 2019; Jiang et al., 2019; Rodovská et al., 2017). Nevertheless, some isotopic systems, including both K and Li, generally show limited variation and no evidence of either evaporative loss or partial condensation (Humayun and Koeberl, 2004; Jiang et al., 2019; Magna et al., 2011; Magna et al., 2021; Rodovská et al., 2016).

With the considerable advances in K isotope analysis (e.g., Wang et al., 2021 and references therein) achieved since the previous K isotope study on microtektites by Herzog et al. (2008), additional K isotope analysis of the Australasian microtektites has the potential to further improve our understanding of microtektite formation. As K is an MVE, it possesses the optimal volatility to be affected by many high temperature processes but is not so volatile to be completely lost. Potassium also has two stable isotopes (^{39}K and ^{41}K) which are in high enough abundance to be measured and fractionate differently depending on the process of depletion (Chen et al., 2019a; Neuman et al., 2022; Yu et al., 2003; Zhang et al., 2021). This combination of properties results in the isotopic analysis of K being ideal for investigating processes of volatile depletion. Additionally, recent improvements in K isotope analysis techniques by multi-collector inductively coupled mass spectrometry (MC-ICP-MS) have opened up many new opportunities, as high-precision K isotope analyses which can distinguish differences down to ~0.1 ‰ is now routinely achievable (Chen et al., 2019b; Hu et al., 2018; Li et al., 2016; Wang and Jacobsen, 2016a).

Here, in order to improve our understanding of both microtektite formation and the formation of other melt droplets (e.g., CB chondrules and lunar impact glasses) during hypervelocity impacts, we undertook elemental and high precision K isotope analysis on microtektites from the Australasian strewn field. Microtektites from this impact present an ideal target for such a study due to the large variability in distances traveled, and thus temperature/time regimes experienced by the microtektites. Australasian microtektites are also the youngest among all microtektites, meaning that they potentially experienced less alteration. Additionally, the already observed volatile depletions and isotopic variations indicate a formation process involving significant variations in volatilization. As shown in Fig. 1, the microtektites selected for this study come from five sites covering a wide range of distances from the proposed impact region. These sites are Ocean Drilling Program (ODP) site 1143A (~1240 km from impact location), ODP site 1144A (~1220 km from impact location), core V19-169 (~4100 km from impact location), core V29-43 (~4800 km from impact location), and Miller Butte (MB) located in Outback Nunataks, Victoria Land, Antarctica (~10,800 km from impact location). All the distance estimates used here are from Folco et al., (2010a) and assume that the source crater location is at 18° N–106° E in the Gulf of Tonkin region (Indochina).

2. Procedure

A total of forty-three microtektites were selected for analysis, consisting of twenty-six specimens from Miller Butte in Antarctica (72.70°S, 160.25°E), five from ODP core site 1143A (9.36°N, 113.29°E), ten from ODP core site 1144A (20.05°N, 117.42°E) and one each from core sites V19-169 (10.22°S, 81.62°E) and V29-43 (12.33°S, 75.08°E), respectively. No microtektites analyzed here were previously irradiated for instrumental neutron activation analysis (INAA). The microtektites analyzed range from 0.111 to 0.662 mg in mass (see Table 1), which equates to ~ 400 to ~700 μm in diameter. The Miller Butte microtektites were similar in shape, colour and texture, with all being pale-yellow, spherically shaped (see Fig. 2 for an optical image), and with no relict

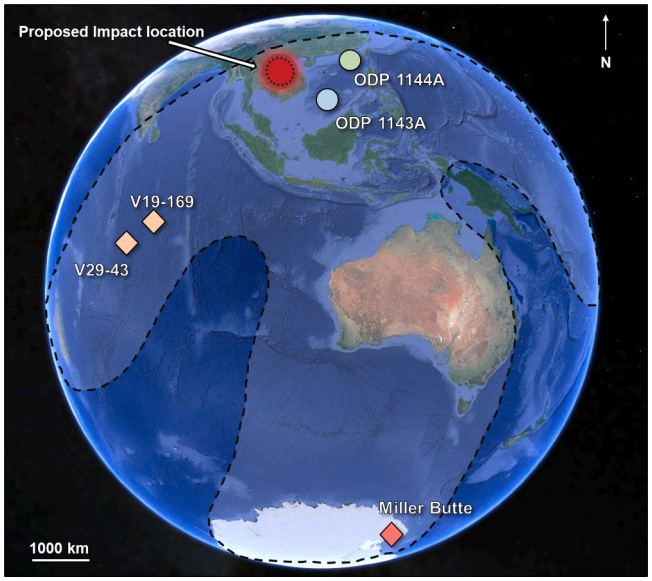

Fig. 1. Map of the Australasian strewn field (dashed line) showing the locations of the microtektites studied here (coloured symbols) and the proposed impact location (red oval) (Burns and Glass, 1989; Glass and Pizzuto, 1994; Hartung, 1990; Hartung and Koeberl, 1994; Ma et al., 2004; Stauffer, 1978). Note the large difference in distance from the impact location of the different microtektite sampling sites.

grains or schlieren. Yet, an individual microbubble was observed in one Miller Butte microtektite. The V19-169 and V29-43 microtektites were also similar to each other, with both being spheres and greenish-yellow with no relict grains or schlieren. The microtektites from the two ODP cores did show more variation, with colours consisting of greenish-yellow (four microtektites), yellowish-brown (three microtektites), and brown (eight microtektites). In terms of shapes, ten of the ODP microtektites were spheres, four were elongate, and one was teardrop shaped. In addition, three ODP microtektites showed highly pitted surfaces (samples 27, 28, and 31), three had some minor vesicles (samples 38, 39, and 40), and one contained a few very small opaque inclusions (sample 39). To remove any possible surface contaminants (some microtektites showed minor amounts of jarosite and gypsum on their surface) each microtektite was ultrasonicated for 5 min in Milli-Q water prior to dissolution. Dissolution of the microtektites was undertaken using 28.9 M Optima™ HF and double-distilled 15.6 M HNO_3 at a 3:1 ratio (1 mL total volume) and heating them to 140 °C for one week. Once dissolution was complete, 10 % of each fraction was reserved for elemental analysis, while the remaining 90 % was used for K isotope analysis.

2.1. Elemental analysis

All elemental analysis undertaken in this study was conducted using a Thermo Fisher iCAP Q ICP-MS at Washington University in St. Louis. Analyses of both the microtektites and Milli-Q leachates were undertaken using KED (kinetic energy discrimination) mode, while the linear calibrations were done using the reference materials BCR-1, BIR-1, BHVO-2, and AGV-1 (Jochum et al., 2016). Additionally, a 5 ppb internal standard of In was run throughout the analysis session. The elemental analysis of the pre-cut, post-cut and K-cut fractions described in section 2.2 were also undertaken using KED mode, however the linear calibrations for these analyses were carried out using a synthetic multi-element solution and no internal standard was used. The precision of the elemental analysis procedure used here is between 2 and 10 % RSD (relative standard deviation).

2.2. Potassium isotope analysis

The separation of K from the matrix was undertaken using a double pass chromatography procedure using Bio-Rad AG50W-X8 100–200 mesh cation-exchange resin. Both passes were conducted using a column with an ID (internal diameter) of 0.5 cm which contained 1.5 mL of resin. Potassium was eluted using 14 mL of 0.5 M HNO_3 while a 1 mL pre-cut and post-cut was collected each side of the K cut to monitor of K loss. For a detailed description of this separation method, albeit using a larger column size, see Chen et al., 2019b. For all samples other than MT16, K loss was found to be negligible (<5%) from the chromatography procedure. For sample MT16, the K loss was significant (30 %), so the K isotope data for this sample is considered compromised and not discussed further. The total procedural blank was 14 ng, which is negligible (<1.5 %) compared to all samples.

The K isotopic analyses of all microtektites were conducted using a Thermo Scientific Neptune *Plus* MC-ICP-MS at Washington University in St. Louis. Analyses were undertaken using the "dry plasma" technique, with an Elemental Scientific APEX Ω high sensitivity desolvating nebulizer used as an introduction system. For detailed description of the "dry plasma" analytical protocol used here see Chen et al., 2020. In brief, analyses were run using a high mass resolution slit (25 μm) and an RF power of 1225 W. All K isotope measurements were taken on the "shoulder" of the ^{41}K peak to avoid interference from the remaining $^{40}ArH^{+}$. In order to correct for instrument mass bias, all measurements were conducted with solutions at 150 ppb K using the sample-standard bracketing technique. The standard used for these analyses was NIST SRM 3141a, with all K isotope data presented in the delta notation $\delta^{41}K = ([(^{41}K/^{39}K)\ \text{sample}/\ (^{41}K/^{39}K)\ \text{standard} - 1] \times 1000)$. The BHVO-2 reference material was analyzed at least once in each analytical session to monitor data quality. From these analyses, a BHVO-2 $\delta^{41}K$ value of -0.47 ± 0.04 ‰ (n = 44) was established, which agrees with previous measurements (Hu et al., 2018; Li et al., 2016; Tuller-Ross et al., 2019; Wang and Jacobsen, 2016a; Wang et al., 2021). The precision of K isotope analyses using this technique over a 20-month period has been evaluated as ± 0.11 ‰ (2 SD) (Chen et al., 2019b), while the 95 % confidence interval within each session is generally ± ~0.05 ‰.

3. Results

3.1. Elemental data

All major and trace element compositions of the microtektites analyzed in this study are listed in Table 2 (all microtektite K concentrations, reported as ppm, are also given in Table 1). As Si cannot be measured using the procedure undertaken here, the reported SiO_2 values in Table 2 are calculated as the total (assumed to be 100 wt%) minus the sum of all the major elements. Overall, the microtektites in this study show similar elemental compositions to other Australasian microtektites, further supporting the consensus that the Transantarctic Mountain microtektites are part of the Australasian microtektite strewn field (Folco et al., 2009; Folco et al., 2010a; Folco et al., 2008). This is most distinctively seen in CaO/MgO versus Al_2O_3/TiO_2 (Fig. 3a) and K_2O/Al_2O_3 versus Na_2O/TiO_2 (Fig. 3b), whereby the microtektites analyzed in this study clearly lie within the same regions as previous Australasian microtektite analyses. All microtektites analyzed in this study fall under the "normal" type (as opposed to the "high-Mg" and "intermediate" types), following the previous chemical classification scheme adopted for Australasian microtektites (Folco et al., 2009; Glass et al., 2004). The highest MgO concentration of 5.52 wt% is found in sample 31 from site V19-169, with all other microtektites showing MgO concentrations < 4.5 wt%.

The K_2O contents of the microtektites analyzed in this study show significant variation, ranging from 0.49 wt% to 3.66 wt% (Table 2). When assessing the microtektites from each individual location the observed K_2O variation is much less, with Miller Butte showing a range

Table 1
Sample information and summary of K isotope and K concentration data for the Australasian microtektties analysed in this study.

Sample name	Locality	Sample weight (mg)	δ^{41}K (‰)	95 % C.I.	n	K (ppm)
1	Miller Butte	0.263	−0.57	0.05	12	10,010
2	Miller Butte	0.388	−0.77	0.05	12	8043
3	Miller Butte	0.306	−0.77	0.09	10	8964
4	Miller Butte	0.368	0.57	0.11	11	9826
5	Miller Butte	0.340	0.13	0.08	9	11,422
6	Miller Butte	0.385	0.10	0.06	11	10,017
7	Miller Butte	0.370	−0.44	0.06	12	11,446
8	Miller Butte	0.165	−0.93	0.07	9	7814
9	Miller Butte	0.222	−2.62	0.12	6	5282
10	Miller Butte	0.172	−1.01	0.04	12	11,214
11	Miller Butte	0.188	−0.60	0.05	11	10,394
12	Miller Butte	0.153	−0.99	0.05	10	10,013
13	Miller Butte	0.138	−0.85	0.06	8	9011
14	Miller Butte	0.152	−1.26	0.08	10	10,327
15	Miller Butte	0.243	−0.71	0.05	12	9178
16	Miller Butte	0.140	−0.93	0.06	8	8659
17	Miller Butte	0.169	−2.58	0.11	8	4199
18	Miller Butte	0.122	−1.11	0.08	10	10,029
19	Miller Butte	0.132	−4.04	0.12	5	4104
20	Miller Butte	0.158	−0.97	0.05	12	9744
21	Miller Butte	0.120	−2.38	0.08	6	6065
22	Miller Butte	0.186	−1.33	0.05	12	10,284
23	Miller Butte	0.179	−1.62	0.06	12	8012
24	Miller Butte	0.130	−1.37	0.04	9	10,001
25	Miller Butte	0.133	−1.74	0.08	9	8015
26	Miller Butte	0.105	−1.71	0.06	9	10,746
27	ODP 1143A	0.234	−0.87	0.08	10	26,499
28	ODP 1143A	0.321	−0.88	0.08	13	27,742
29	ODP 1143A	0.241	−0.44	0.05	12	22,417
30	ODP 1143A	0.141	−1.06	0.07	10	26,443
31	ODP 1143A	0.205	−0.66	0.08	9	26,776
32	ODP 1144A	0.148	−0.67	0.10	7	24,822
33	ODP 1144A	0.182	−0.21	0.07	9	29,630
34	ODP 1144A	0.200	−0.45	0.08	9	23,888
35	ODP 1144A	0.111	−1.05	0.06	10	24,399
36	ODP 1144A	0.135	−0.98	0.04	10	23,692
37	ODP 1144A	0.174	−0.57	0.07	11	20,618
38	ODP 1144A	0.224	−0.54	0.10	10	25,330
39	ODP 1144A	0.193	−0.53	0.07	9	27,662
40	ODP 1144A	0.138	−0.97	0.06	10	25,015
41	ODP 1144A	0.662	−0.51	0.09	10	30,404
42	V19-169	0.135	−2.29	0.13	5	7847
43	V29-43	0.133	0.11	0.06	9	12,070

All K isotope data in was onbtained by MC-ICP-MS, while all K concentration data obtained by Q-ICP-MS.
The K concentraion data presented here can also be seen reported as K_2O in Table 2.

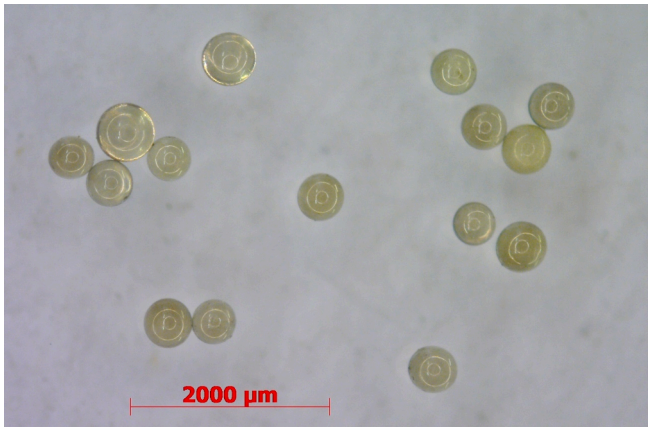

Fig. 2. Optical image showing fifteen representative Australasian microtektites analyzed in this study. All shown microtektites were collected from Miller Butte located within Outback Nunataks, Victoria Land, Antarctica. Note that all fifteen microtektites are spherical, with limited features, and appear near identical in colour, which is unusual as microtektites often show shape, texture, and colour variations.

from 0.49 wt% to 1.38 wt%, ODP 1143A displaying a range from 2.70 wt % to 3.34 wt%, ODP 1144A exhibiting a range from 2.48 wt% to 3.66 wt %, and V19-169 and V29-43 having concentrations of 0.95 wt% and 1.45 wt% respectively. As shown in Fig. 4A, these observed concentration ranges for each site agree with previous data and indicate that the microtektites more distal from the proposed impact site have lower K concentrations (Folco et al., 2010a; Glass et al., 2004; Glass and Koeberl, 2006). Compared to the mean K_2O content of 2.80 wt% estimated for the UCC (Rudnick and Gao, 2014), the microtektites show concentrations from slightly higher to significantly lower. The concentrations of other MVE show a similar pattern to K, nonetheless, Na is significantly depleted in all microtektites (Table 2) relative to the bulk crustal composition of 3.27 wt% (Rudnick and Gao, 2014), whereas K is only significantly depleted in the microtektites distal from the proposed impact region. Interestingly, U, which is generally considered refractory, shows a similar depletion pattern to K (Table 2). This, however, has been noted before by previous studies and is explained as U behaving volatile during microtektite formation due to high pO_2 and the siting of U in reduced carbonaceous material of the host rock (Folco et al., 2009; Van Ginneken et al., 2018; Wasson et al., 1990).

Table 2
Major and trace element abundances of Australasian microtektites analyzed in this study.

Sample No.	1	2	3	4	5	6	7	8	9	10	11	12	13	14	15
Locality	MB	MB	MB	MB	MB	MB	MB	MB	MB	MB	MB	MB	MB	MB	MB
Average [wt %]															
[a]SiO_2	72.1	64.6	74.2	77.6	70.8	74.7	76.0	74.1	69.5	71.1	71.6	72.4	77.7	75.6	75.6
TiO_2	0.82	1.02	0.77	0.72	0.88	0.78	0.73	0.80	0.94	0.88	0.86	0.83	0.70	0.76	0.76
Al_2O_3	14.60	18.54	13.40	12.53	15.91	13.50	12.53	14.21	16.33	16.09	15.63	15.56	12.33	13.15	13.34
FeO	4.33	4.50	3.93	2.83	4.50	3.61	3.92	3.23	3.40	4.31	4.17	3.87	2.56	3.57	3.43
MnO	0.09	0.10	0.08	0.07	0.09	0.08	0.08	0.08	0.09	0.09	0.09	0.09	0.06	0.08	0.08
MgO	3.31	3.82	2.91	1.96	2.73	2.38	2.53	2.98	4.29	2.87	2.77	2.67	2.12	2.19	2.26
CaO	3.31	6.10	3.45	2.93	3.51	3.60	2.65	3.61	4.71	3.23	3.54	3.38	3.38	3.17	3.24
Na_2O	0.31	0.41	0.26	0.31	0.34	0.28	0.30	0.31	0.26	0.38	0.35	0.34	0.36	0.34	0.28
K_2O	1.21	0.97	1.08	1.18	1.38	1.21	1.38	0.94	0.64	1.35	1.25	1.21	1.09	1.24	1.11
[ppm]															
Li	45.6	47.9	43.0	27.5	52.1	37.2	46.9	29.6	36.4	54.7	49.0	52.6	33.6	38.3	36.3
Be	2.71	1.83	1.57	2.91	3.00	2.51	2.48	3.50	2.78	3.03	3.02	1.87	0.70	2.53	3.06
Sc	14.3	20.1	12.3	12.4	15.3	12.5	12.0	15.0	15.7	16.0	14.1	14.8	10.3	13.2	11.9
V	33.1	32.0	26.4	27.8	38.8	31.7	28.4	27.1	18.3	34.6	34.9	30.3	27.6	30.3	27.1
Cr	54.8	54.6	64.9	37.4	48.3	59.2	63.7	42.0	75.5	40.3	38.4	50.9	37.2	41.6	51.7
Co	6.92	5.96	9.46	4.44	6.59	7.90	7.12	3.28	3.47	9.59	13.20	6.75	1.67	5.60	4.76
Ni	9.5	18.3	60.0	4.5	6.7	7.6	9.2	9.1	9.4	10.8	10.6	6.9	9.0	6.5	5.4
Cu	0.10	3.39	0.10	b.d.	1.40	0.16	0.10	1.11	5.97	1.68	2.71	0.52	0.10	0.44	b.d.
Zn	20.4	34.8	16.2	33.6	21.3	0.2	0.1	4.4	30.3	24.4	0.1	5.0	177.1	4.5	b.d.
Ga	9.99	11.75	8.40	9.32	10.14	9.17	9.34	9.77	11.39	10.70	10.40	9.67	8.45	9.28	8.13
Rb	50.9	38.3	43.9	52.0	61.6	51.3	55.8	37.9	21.3	59.1	54.8	52.0	44.0	51.8	46.7
Sr	187	252	205	202	201	210	170	218	274	191	197	201	196	198	209
Y	36.6	45.8	38.1	34.9	38.7	35.6	33.3	37.0	43.6	39.2	36.7	37.8	31.8	32.6	33.4
Zr	318	341	342	343	317	338	319	358	421	342	294	324	335	292	312
Nb	20.0	21.9	20.6	18.1	19.9	18.1	18.3	20.1	22.4	20.8	19.8	16.3	18.2	19.6	18.6
Cs	2.36	1.79	1.90	2.28	3.32	2.24	2.59	1.55	1.02	2.85	2.86	2.48	2.37	2.34	2.19
Ba	491	601	486	549	492	499	471	538	628	519	500	531	492	483	499
La	48.3	59.4	46.7	46.5	50.1	47.2	44.5	49.3	57.9	51.0	49.3	50.4	43.1	45.4	45.8
Ce	95.0	117.1	91.0	88.7	97.8	92.7	87.4	96.4	115.0	100.1	97.5	98.7	82.5	88.3	89.5
Pr	10.7	13.6	10.6	10.4	11.4	10.8	10.0	11.0	13.1	11.4	11.1	11.3	9.8	10.3	10.5
Nd	41.7	51.2	39.8	39.2	42.8	40.6	37.6	42.4	49.4	44.3	42.4	42.7	36.9	37.8	39.5
Sm	8.11	9.62	8.16	7.24	8.20	7.68	7.26	7.90	9.73	8.44	7.76	7.94	6.72	7.76	7.21
Eu	1.45	1.87	1.50	1.39	1.54	1.34	1.34	1.53	1.70	1.58	1.56	1.58	1.26	1.29	1.42
Gd	7.02	8.58	7.06	6.65	7.46	6.76	6.57	7.09	8.15	7.60	7.31	7.21	6.16	6.32	6.69
Tb	1.03	1.34	1.12	1.00	1.12	1.02	0.95	1.09	1.32	1.11	1.06	1.09	0.95	1.02	1.02
Dy	6.21	7.63	6.52	5.63	6.61	5.94	5.56	6.37	7.40	6.69	5.99	6.37	5.39	5.86	5.97
Ho	1.26	1.51	1.29	1.13	1.31	1.17	1.11	1.29	1.40	1.32	1.22	1.24	1.07	1.09	1.16
Er	3.53	4.27	3.71	3.36	3.82	3.42	3.28	3.66	4.18	3.97	3.64	3.65	2.91	3.32	3.32
Tm	0.57	0.68	0.59	0.53	0.62	0.54	0.51	0.56	0.65	0.62	0.59	0.61	0.49	0.51	0.56
Yb	3.43	4.30	3.52	3.20	3.90	3.37	3.17	3.50	4.05	3.52	3.46	3.54	3.23	3.12	3.22
Lu	0.54	0.62	0.52	0.47	0.54	0.49	0.47	0.47	0.56	0.55	0.55	0.56	0.45	0.43	0.45
Hf	8.20	9.04	8.69	9.01	8.22	8.69	8.13	9.33	10.78	8.30	7.84	8.11	8.60	8.29	8.68
Ta	1.45	1.33	1.34	1.29	1.10	1.09	1.25	1.48	1.56	1.50	1.27	0.63	1.31	1.55	1.45
Pb	0.45	4.93	0.45	0.40	0.30	0.38	0.23	0.73	0.41	0.42	4.25	0.24	1.22	0.88	0.17
Th	17.1	20.6	16.7	16.0	19.0	16.8	15.7	17.6	20.3	18.7	17.9	17.9	14.9	16.5	16.9
U	0.66	0.56	0.61	0.86	1.82	0.84	0.74	0.60	0.30	0.62	0.61	0.57	0.75	0.88	0.78
Sample No.	**16**	**17**	**18**	**19**	**20**	**21**	**22**	**23**	**24**	**25**	**26**	**27**	**28**	**29**	**30**
Locality	**MB**	**MB**	**MB**	**MB**	**MB**	**MB**	**MB**	**MB**	**MB**	**MB**	**MB**	**1143A**	**1143A**	**1143A**	**1143A**
Average [wt %]															
[a]SiO_2	69.6	63.4	69.6	67.5	71.0	66.3	74.6	71.4	70.8	78.0	72.1	63.3	64.0	70.0	63.1
TiO_2	0.92	1.16	0.93	0.96	0.88	1.07	0.79	0.84	0.90	0.69	0.88	0.94	0.94	0.76	1.01
Al_2O_3	16.68	21.55	16.88	16.39	15.94	19.19	13.84	14.47	16.29	11.72	15.41	19.60	19.11	13.29	20.74
FeO	4.36	4.06	4.54	4.22	4.27	4.22	3.66	4.92	4.29	3.23	3.95	6.24	6.22	5.77	6.30
MnO	0.09	0.10	0.09	0.11	0.09	0.10	0.08	0.10	0.09	0.07	0.09	0.12	0.09	0.10	0.09
MgO	2.88	4.20	2.83	5.46	2.72	3.76	2.21	3.89	2.71	2.39	2.76	2.86	2.73	3.37	2.89
CaO	4.31	4.89	3.72	4.69	3.69	4.46	3.38	3.18	3.47	2.71	2.93	2.79	2.47	2.54	1.80
Na_2O	0.30	0.18	0.37	0.27	0.34	0.24	0.30	0.33	0.38	0.32	0.71	1.13	1.19	1.52	1.17
K_2O	1.043	0.506	1.208	0.494	1.174	0.731	1.239	0.965	1.205	0.965	1.294	3.192	3.342	2.70	3.19
[ppm]															
Li	47.9	49.6	52.9	28.1	45.1	54.0	39.8	36.4	53.9	26.9	39.4	113.5	122.3	71.6	133.3
Be	1.22	5.30	2.00	3.95	0.60	7.98	2.41	0.42	0.68	0.55	2.18	4.30	1.68	2.17	3.76
Sc	15.5	22.7	16.7	14.1	16.4	21.4	14.0	14.3	16.7	13.6	13.8	17.4	15.7	12.0	17.5
V	40.1	26.7	47.8	19.9	38.0	30.9	30.0	29.1	42.0	25.0	35.0	113.9	108.9	92.0	97.4
Cr	44.6	140.8	37.7	215.5	34.2	51.8	39.2	99.2	35.3	43.1	47.3	91.9	93.4	254.1	87.4
Co	5.02	4.82	4.25	5.68	5.04	3.32	4.70	7.57	4.39	4.13	4.56	15.91	17.68	36.47	11.65
Ni	6.6	36.3	4.6	15.6	7.6	4.4	4.1	24.1	5.4	4.2	7.9	26.0	29.8	408.4	29.0
Cu	6.03	4.67	b.d.	0.45	0.67	b.d.	b.d.	b.d.	b.d.	5.06	6.25	23.49	5.73	4.97	10.12
Zn	38.9	0.5	b.d.	297.0	b.d.	b.d.	b.d.	b.d.	b.d.	180.2	28.9	16.4	1.2	0.1	28.6

(*continued on next page*)

Table 2 (*continued*)

Ga	8.76	12.33	11.28	10.97	11.09	10.03	10.03	10.32	9.54	6.83	10.84	12.26	11.88	12.11	11.10
Rb	49.4	20.6	58.4	16.1	56.1	31.5	50.6	41.3	58.9	40.8	53.1	148.7	158.9	122.8	134.0
Sr	233	263	214	260	212	241	207	186	206	165	191	156	150	134	160
Y	36.0	48.2	37.9	41.7	37.5	41.1	34.3	36.8	37.6	29.0	37.9	34.5	36.0	31.1	38.8
Zr	281	344	276	406	293	313	326	326	282	298	349	198	203	261	246
Nb	22.1	26.4	21.4	22.6	21.6	24.4	20.3	21.2	22.0	16.7	22.1	20.0	22.2	16.8	22.4
Cs	2.79	0.97	3.60	0.81	3.21	1.44	2.37	1.94	3.42	2.01	2.62	8.17	9.15	6.14	7.18
Ba	518	680	522	628	518	611	517	502	511	421	529	510	502	416	533
La	50.5	64.3	50.3	57.0	50.1	57.7	47.1	48.8	49.5	40.1	51.2	51.7	51.0	41.5	54.5
Ce	99.5	125.7	100.4	114.8	97.9	116.1	92.9	96.2	98.5	78.3	100.9	104.5	103.9	83.9	109.6
Pr	11.5	14.8	11.4	12.6	11.2	13.3	10.9	11.1	11.6	9.1	11.9	11.5	11.6	9.6	12.1
Nd	43.9	56.6	43.8	48.0	41.9	51.1	41.1	41.8	43.1	34.1	45.9	42.9	43.5	34.8	45.2
Sm	8.36	11.01	8.42	9.39	8.15	9.86	7.39	8.07	8.42	6.99	8.50	8.43	8.42	6.51	8.74
Eu	1.63	2.13	1.58	1.80	1.64	1.91	1.42	1.48	1.68	1.19	1.62	1.69	1.65	1.27	1.75
Gd	7.55	9.96	7.66	8.77	7.68	9.19	7.21	7.62	7.53	6.29	7.97	7.23	7.45	6.32	7.65
Tb	1.18	1.48	1.22	1.25	1.15	1.28	1.09	1.11	1.18	0.89	1.19	1.06	1.09	0.96	1.14
Dy	6.75	8.24	6.45	7.03	6.41	7.13	5.78	6.31	6.56	5.23	6.47	6.12	6.21	5.53	6.30
Ho	1.27	1.61	1.29	1.47	1.25	1.43	1.19	1.25	1.23	1.03	1.28	1.22	1.20	1.06	1.33
Er	3.73	4.62	3.91	4.07	3.58	4.11	3.28	3.49	3.82	2.96	3.65	3.62	3.57	2.98	3.85
Tm	0.57	0.76	0.64	0.67	0.57	0.69	0.56	0.56	0.60	0.45	0.59	0.57	0.56	0.51	0.61
Yb	3.56	4.64	3.69	4.19	3.63	4.16	3.39	3.37	3.41	2.65	3.86	3.31	3.25	3.01	3.73
Lu	0.54	0.70	0.52	0.59	0.56	0.58	0.50	0.53	0.50	0.47	0.61	0.52	0.51	0.47	0.52
Hf	8.09	9.69	7.82	11.47	8.23	8.64	9.25	9.17	8.14	8.08	9.60	5.20	5.56	6.82	6.16
Ta	1.66	2.07	1.76	1.81	1.58	1.94	1.63	1.67	1.51	1.38	1.96	1.20	1.33	1.23	1.62
Pb	0.25	6.66	0.13	b.d.	0.26	b.d.	0.04	0.82	0.03	0.39	0.79	5.30	1.35	3.29	1.58
Th	19.5	25.0	19.5	21.3	19.0	22.5	17.8	18.0	19.2	15.2	19.1	19.8	20.2	14.8	21.4
U	0.79	0.38	1.07	0.30	0.87	0.51	0.94	0.56	0.92	0.56	0.80	2.65	2.78	2.65	2.01

Sample No.	**31**	**32**	**33**	**34**	**35**	**36**	**37**	**38**	**39**	**40**	**41**	**42**	**43**
Locality	**1143A**	**1144A**	**1144A**	**1144A**	**1144A**	**1144A**	**1144A**	**1144A**	**1144A**	**1144A**	**1144A**	**V19-169**	**V29-43**
Average [wt %]													
[a]SiO_2	64.0	72.2	61.8	62.6	72.4	71.4	69.8	68.7	63.1	68.0	62.4	68.6	72.3
TiO_2	0.92	0.80	0.92	0.99	0.78	0.71	0.80	0.85	0.93	0.83	0.93	0.82	0.72
Al_2O_3	19.11	13.26	19.37	20.61	13.37	12.31	14.63	15.05	19.59	16.12	19.36	14.58	13.13
FeO	6.26	4.69	6.82	6.18	4.58	5.44	4.95	5.25	6.49	5.42	6.45	5.37	5.27
MnO	0.09	0.09	0.10	0.09	0.09	0.10	0.10	0.09	0.08	0.09	0.08	0.11	0.10
MgO	2.86	2.11	3.17	2.97	2.48	2.97	2.41	2.49	2.98	2.63	2.85	5.38	3.57
CaO	2.52	2.42	2.91	2.95	1.80	2.76	3.71	3.05	2.47	2.78	2.85	3.96	3.27
Na_2O	1.21	1.69	1.48	0.92	1.84	1.61	1.42	1.55	1.24	1.33	1.37	0.46	0.43
K_2O	3.23	2.99	3.57	2.88	2.94	2.85	2.48	3.05	3.33	3.01	3.66	0.95	1.45
[ppm]													
Li	118.3	72.0	120.6	125.2	90.3	68.9	75.1	84.7	123.7	99.8	125.4	33.9	37.0
Be	3.70	1.26	4.22	3.33	3.87	2.52	2.50	2.15	4.44	1.71	3.47	3.48	0.72
Sc	17.7	11.7	18.4	16.9	10.7	12.0	15.7	14.2	18.0	14.2	17.4	15.1	12.0
V	113.6	92.4	136.5	111.9	92.8	88.1	69.4	101.8	122.2	99.8	133.2	38.5	49.1
Cr	91.6	69.6	101.0	97.3	80.5	227.6	55.1	71.9	96.1	71.4	97.4	213.9	158.9
Co	14.1	12.0	17.9	23.8	35.1	34.5	14.7	19.0	29.1	11.2	18.2	13.0	20.6
Ni	23.4	35.0	35.0	19.7	44.8	173.8	25.1	34.2	24.3	21.3	45.3	36.6	50.5
Cu	19.65	9.47	8.05	8.37	16.69	4.26	2.90	6.71	8.03	140.48	8.55	0.58	2.15
Zn	1.1	18.9	28.0	17.7	52.1	0.1	2.0	54.8	55.8	42.5	229.0	254.6	42.3
Ga	12.89	17.87	18.96	13.30	16.59	13.02	11.17	19.58	15.29	17.32	20.17	8.86	8.05
Rb	151.0	138.0	176.4	134.8	137.1	123.6	104.2	144.0	162.2	139.3	187.4	35.9	66.7
Sr	149	138	151	163	161	151	193	153	150	151	158	198	176
Y	34.2	32.8	34.4	37.8	36.2	30.7	34.3	34.3	35.7	34.0	34.5	35.4	30.1
Zr	203	268	197	219	285	259	255	265	199	238	194	289	260
Nb	20.7	18.8	19.6	22.4	18.6	16.5	18.9	19.0	17.3	18.2	20.6	19.1	16.3
Cs	8.73	7.44	10.96	8.05	6.77	6.09	5.17	8.07	9.35	7.39	11.70	1.67	3.43
Ba	500	430	530	527	443	397	448	450	505	476	502	466	418
La	49.0	41.9	48.3	54.2	44.8	39.4	44.8	45.6	50.3	45.1	50.4	45.1	40.5
Ce	99.7	85.5	98.4	110.8	90.3	80.5	90.0	93.4	103.2	91.2	101.8	89.8	81.1
Pr	11.2	9.6	11.0	12.4	10.3	8.8	10.3	10.6	11.6	10.0	11.4	10.2	9.3
Nd	42.2	35.7	41.6	45.8	37.9	34.1	38.4	39.2	42.8	38.6	42.3	38.8	35.3
Sm	7.84	7.01	7.92	8.65	6.92	6.26	7.20	7.18	8.17	7.04	8.09	7.26	7.07
Eu	1.50	1.28	1.60	1.72	1.22	1.18	1.40	1.52	1.53	1.47	1.56	1.59	1.32
Gd	7.07	6.29	7.00	7.76	6.18	6.07	6.73	7.08	6.88	6.83	7.25	6.97	6.02
Tb	1.06	0.90	1.09	1.15	0.98	0.87	0.97	1.03	1.05	1.03	1.05	1.07	0.90
Dy	6.06	5.77	5.79	6.50	5.59	4.96	5.74	6.08	6.08	5.72	6.00	5.98	5.18
Ho	1.20	1.09	1.19	1.32	1.10	0.95	1.13	1.16	1.20	1.09	1.21	1.23	1.01
Er	3.40	3.16	3.28	3.77	3.33	2.77	3.28	3.35	3.49	3.09	3.46	3.20	2.83
Tm	0.56	0.49	0.52	0.63	0.49	0.51	0.53	0.52	0.55	0.53	0.53	0.57	0.45
Yb	3.42	3.02	3.41	3.65	3.22	2.79	3.10	3.19	3.46	3.23	3.25	3.33	2.97
Lu	0.47	0.41	0.46	0.50	0.45	0.44	0.50	0.48	0.49	0.45	0.47	0.50	0.41
Hf	5.40	7.00	5.39	5.90	7.56	6.66	6.46	7.02	5.20	6.38	5.26	7.69	6.53
Ta	1.37	1.23	1.30	1.53	3.12	1.23	1.52	1.35	0.79	1.30	1.42	1.34	0.06
Pb	1.26	11.50	10.61	4.58	24.93	9.23	3.07	20.06	16.52	16.90	15.03	0.88	1.04
Th	18.8	15.3	18.5	21.4	15.1	13.8	16.2	16.6	19.5	16.7	20.2	16.5	14.5
U	2.64	2.74	3.66	2.74	2.72	2.40	1.81	3.23	3.22	2.41	3.93	0.56	1.12

All elemental data in Table 2 obtained by Q-ICP-MS. The relative standard deviation of this analysis procedure is 2–10%.
[a]SiO2 = total – sum of major elements, where total is assumed to be 100 wt%.
b.d. = below detection limit.
MB = Miller Butte microtektties.
1143A = ODP site 1143A microtektties.
1144A = ODP site 1144A microtektties.

3.2. Potassium Isotope Data

The K isotope compositions of all Australasian microtektites analyzed in this study are listed in Table 1. The total observed $\delta^{41}K$ range of the microtektites studied here is from –4.04 ± 0.12 ‰ to 0.57 ± 0.11 ‰ (unless otherwise stated, all $\delta^{41}K$ uncertainties reported are as 95 % CI). Interestingly, as shown in Fig. 4B, this entire range is dictated by the Miller Butte microtektites, with the ODP 1143A and ODP 1144A microtektites spanning the more restricted $\delta^{41}K$ ranges of –1.06 ± 0.07 ‰ to –0.44 ± 0.05 ‰ and −1.05 ± 0.06 ‰ to − 0.21 ± 0.07 ‰, respectively. The V19-169 microtektite and V29-43 microtektite have $\delta^{41}K$ values of –2.29 ± 0.13 ‰ and 0.11 ± 0.06 ‰ respectively. Compared to the $\delta^{41}K$ value of − 0.42 ± 0.17 ‰ estimated for the Bulk Silicate Earth (BSE) (Tuller-Ross et al., 2019; Wang and Jacobsen, 2016a), the ODP microtektites span from the BSE value to slightly lighter (excluding one sample), while microtektites from the other sites cover ranges both heavier and lighter than the BSE.

When compared to K concentration, represented as $1/K_2O$ in Fig. 5A, the microtektites define two different groups, (i) the OPD microtektites with high K concentrations and narrow K isotope variation, and (ii) the Miller Butte, V19-169, and V29-43 microtektites with low K concentrations and large K isotope variation. There appears to be a correlation among specimens from the latter group whereby the lower-K microtektites have lighter K isotope compositions, nevertheless this correlation is largely dictated by five samples. In contrast, the ODP microtektite group shows limited K concentration variation resulting in a near vertical trend. As seen in Fig. 5B, C, and D, when K isotope composition is compared against a relative K depletion factor expressed as Al/K, Ti/K, and Mg/K, similar patterns are observed to what is seen for $1/K_2O$ (to see Fig. 5 data plotted without the reciprocal use of K concentration, i.e., with the x axis as K_2O, K/Al, K/Ti, and K/Mg, see Supplementary Fig. 1).

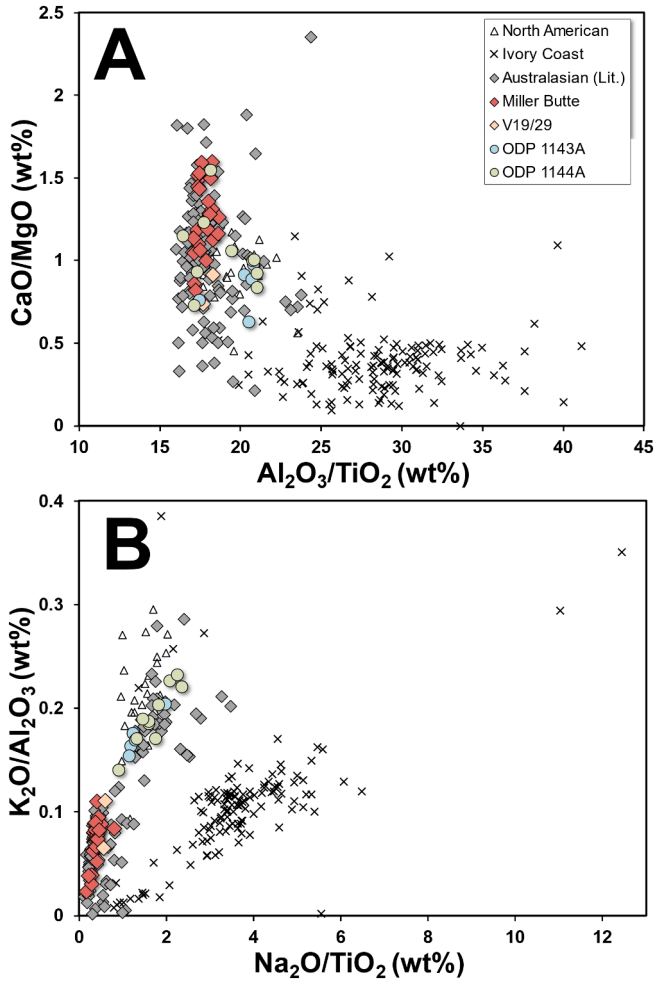

Fig. 3. Plots of (A) CaO/MgO vs Al_2O_3/TiO_2 and (B) K_2O/Al_2O_3 vs Na_2O/TiO_2 for all Australasian microtektites analyzed in this study. For comparison, a range of data for North American, Ivory Coast, and Australasian microtektite data from other sources is also plotted Folco et al., 2009; Glass et al., 2004; Glass and Koeberl, 2006; Koeberl et al., 1997). As shown, all microtektites studied here lie within the range seen among other Australasian microtektites. Also note the significant K and Na depletions seen among the Miller Butte and V19/29 microtektites shown in (B). V19/29 refers to the single microtektites from cores V19-169 and V29-43.

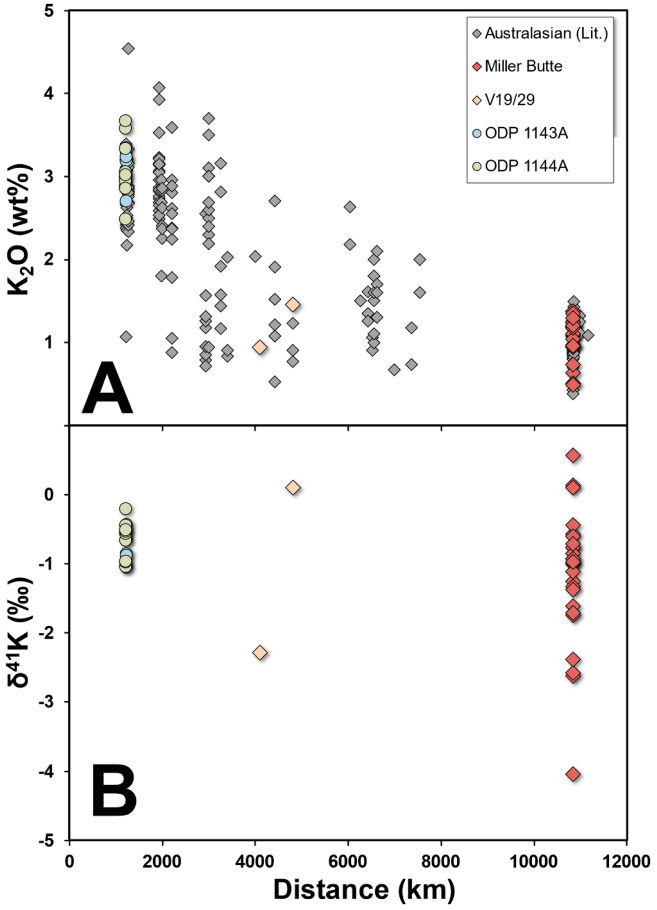

Fig. 4. Plots of distance from putative source region verses K_2O (A) and K isotope composition (B) for Australasian microtektites. The literature data plotted in A are from Folco et al. (2009), Folco et al., (2010a), Folco et al., (2010b), Glass et al. (2004) Glass and Koeberl (2006). The distance estimates are from Folco et al., (2010a). As shown in (A), K_2O concentrations both decrease and show less variation with distance, while as seen in (B), microtektite $\delta^{41}K$ values become broadly lower and more variable with distance. V19/29 refers to the single microtektites from cores V19-169 and V29-43.

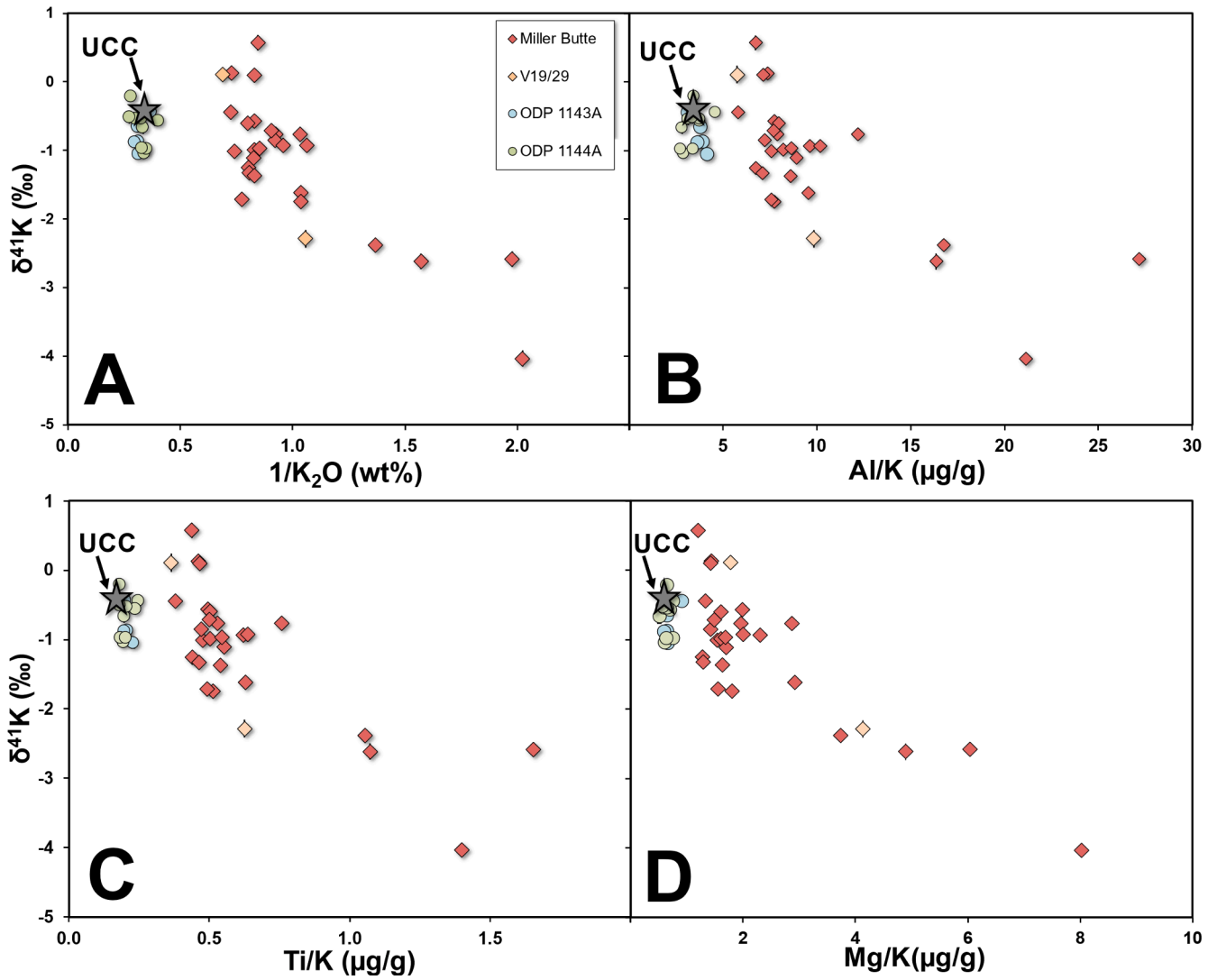

Fig. 5. Plots showing K isotope composition of all microtektites analyzed in this study vs. (A) $1/K_2O$, (B) Al/K, (C) Ti/K, and (D) Mg/K. The UCC composition is also shown for comparison as a grey star (Rudnick and Gao, 2014; Tuller-Ross et al., 2019). Uncertainties shown for $\delta^{41}K$ are 95 % CI. As shown in all plots, more K-depleted microtektites show lighter K isotope compositions. Additionally, the Miller Butte and V19/29 microtektites are overall more K depleted and show significantly greater $\delta^{41}K$ variation. V19/29 refers to the single microtektites from cores V19-169 and V29-43.

4. Discussion

4.1. Potassium isotope compositions of australasian microtektites

4.1.1. This study

The Australasian microtektites analyzed in this study cover a total $\delta^{41}K$ range of ~4.5 ‰, which, when compared to all previous bulk K isotope samples analyzed is substantial, as all bulk Earth rocks, bulk chondrites (and chondrules), and bulk achondrites show total $\delta^{41}K$ ranges of ~2 ‰ or less (Bloom et al., 2020; Koefoed et al., 2020; Koefoed et al., 2022; Koefoed et al., 2023; Ku and Jacobsen, 2020; Nie et al., 2021; Nie et al., 2023; Parendo et al., 2017; Tian et al., 2019; Tian et al., 2021; Tuller-Ross et al., 2019; Wang and Jacobsen, 2016a, 2016b; Wang et al., 2021). This strongly suggests that the K isotope compositions of these microtektites were significantly fractionated from their corresponding precursor compositions during their formation. Nevertheless, as most prominently seen in Fig. 4, there appears to be a stark difference between the microtektites which travelled far from the proposed impact site, and those that landed close, with the far travelled microtektites covering the entire ~4.5 ‰ range and the short travelled microtektites covering a ~0.8 ‰ range. As such, the microtektites analyzed in this study can be split into two distinct groups, 1) the"ODP group" representing the microtektites which display limited $\delta^{41}K$ variation, high K concentrations, and landed closer to the proposed impact site, and 2) the "MB group" (referencing the Miller Butte microtektites which dominate this sample grouping) representing the microtektites with large $\delta^{41}K$ variation, low K concentrations, and which landed further from the proposed impact site. This grouping is most likely somewhat of an oversimplification, as the K concentration data of all Australasian microtektites (Figs. 3 and 4) indicates there is more of a continuum rather than two groups. Yet, as the microtektites analyzed here essentially represent the two endmembers, assigning two distinct groups is considered appropriate for this study.

While the two microtektite groups investigated here show many differences, both groups do show some broad similarities. Firstly, both groups show $\delta^{41}K$ values both above and below the BSE value of –0.43 ± 0.17 ‰ (2SD) (Tuller-Ross et al., 2019), albeit the ODP group only has one microtektite which is slightly above this value (–0.21 ± 0.07 ‰). Secondly, as shown in Fig. 6A-B, both groups show a broad correlation between $\delta^{41}K$ and microtektite mass, with the smaller microtektites having lighter $\delta^{41}K$ compositions (note: sample 41 is excluded from Fig. 6A as it is both significantly larger than all other microtektites

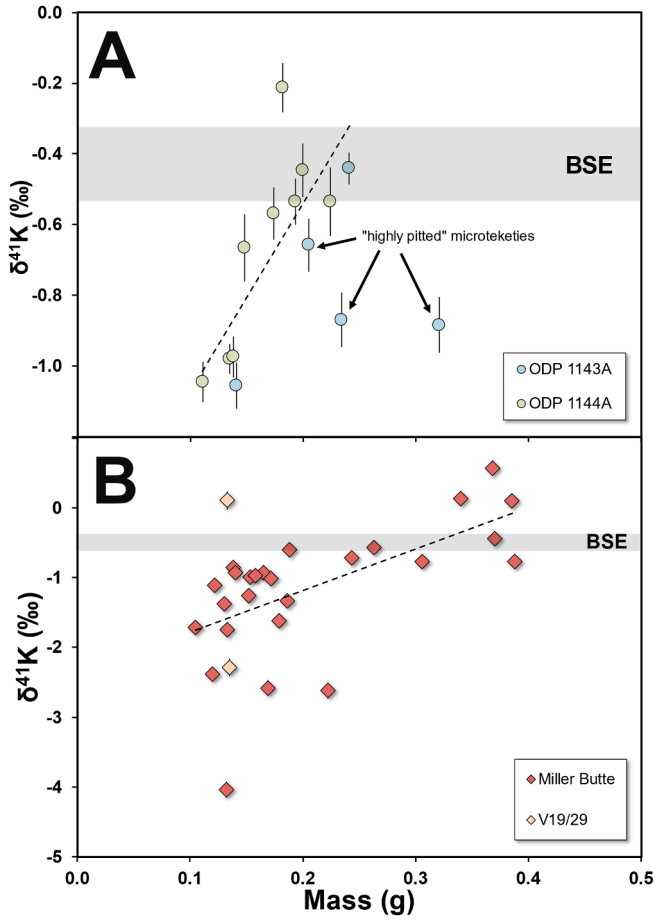

Fig. 6. Plots showing K isotope composition against mass for (A) the ODP group microtektites and (B) the MB group microtektites. The BSE K isotope composition is also shown for comparison (Tuller-Ross et al., 2019). Uncertainties shown for $\delta^{41}K$ are 95 % CI. Note the broad correlation seen for both groups of microtektites, which also show similar slopes (ODP group = 5.33 ± 2.76, MB group = 5.97 ± 3.50, slope uncertainties are 2SE). V19/29 refers to the single microtektites from cores V19-169 and V29-43.

analyzed in this study and is a fragment). For the ODP group, this trend is also stronger when the three microtektites with "highly pitted" textures are excluded, which is not surprising as these textures could be a result of surface etching in sea water or evaporation during their formation both of which could impact $\delta^{41}K$ composition (K is both moderately volatile and fluid mobile). Interestingly, both groups show similar slopes (ODP group = 5.33 ± 2.76, MB group = 5.97 ± 3.50, slope uncertainties are 2SE), suggesting a common mechanism could have produced this trend. As the smaller microtektites show lighter K isotopic compositions, this could indicate incomplete condensation under a kinetic fractionation dominant regime, as less condensation would result in a smaller mass overall, while less condensation of K would result in a lower $\delta^{41}K$ value. As shown in Fig. 5, this also agrees with the K depletion trends, as the more K depleted microtektites show lighter K isotope compositions, consistent with condensation experiments conducted on K originally designed for studying chondrule formation (Georges et al., 2000). Nevertheless, several microtektites show K isotope compositions which are heavier than the BSE composition and have much lower K concentrations (specifically among the MB group). This indicates that if condensation was the dominant formation process for these microtektites, the starting K composition for these microtektites could be different from the bulk UCC composition. Alternatively, it is possible that the uptake of a light vapor regulated by surface to mass ratio (resulting in the smaller microtektites incorporating isotopically lighter vapor as a percentage of their overall mass) could explain the observed $\delta^{41}K$ and microtektite mass correlation. Yet, if this was the case the smaller microtektites would likely be enriched in K relative to the larger microtektites which is the opposite to what is observed (unless the larger microtektites were significantly more enriched in ^{41}K prior to uptake of the isotopically light-K vapor).

4.1.2. *Comparison with previous data*

Although the microtektites analyzed in this study cover a large range, as shown in Fig. 7, the previous Australasian microtektite K isotope data from Herzog et al. (2008), cover a much wider range, with their analyses ranging from –11.0 to 14.3 ‰ (relative to NIST SRM 3141a). The reason for this difference is not entirely clear, however, the analyses by Herzog et al. (2008) were undertaken *in situ* using ion microprobe, as opposed to the bulk analyses using MC-ICP-MS conducted here. The typical analytical precision for K isotope analyses using ion microprobe is 0.5–1 ‰ (Herzog et al., 2008; Alexander and Grossman, 2005; Alexander et al., 2000), while the recently developed MC-ICP-MS method shows precision of 0.05–0.1 ‰ (e.g., Chen et al., 2019b; Hu et al., 2018; Li et al., 2016; Wang and Jacobsen, 2016a). This indicates that while variance in analytical precision could account for some of these observed differences, it cannot account for the majority. The large K isotope variation from Herzog et al. (2008) could indicate that these microtektites contain significant internal K isotope heterogeneities, with the *in situ* analyses capable of highlighting this. Yet,

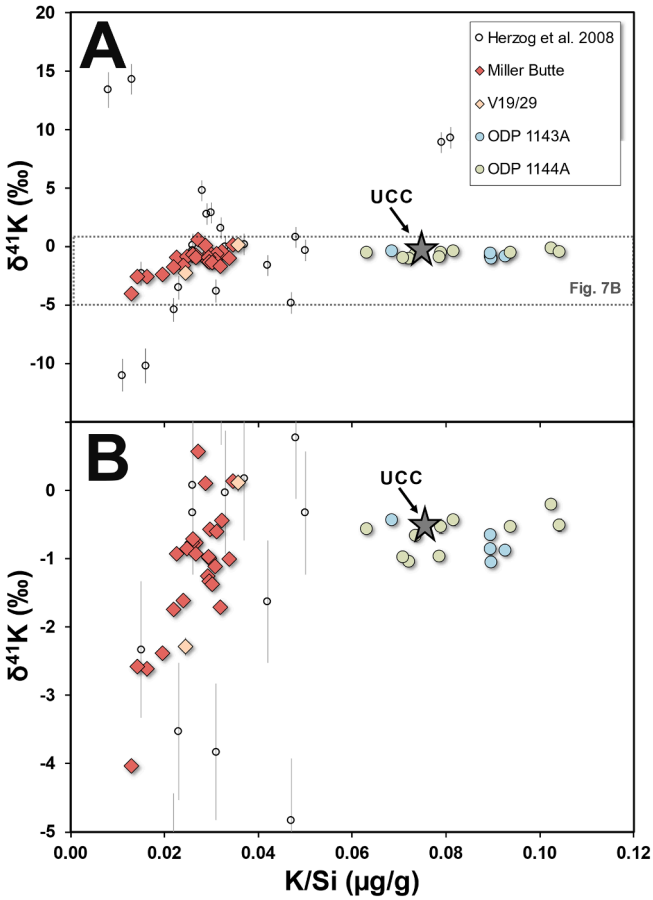

Fig. 7. Plots showing K isotope composition vs K/Si for microtektites analyzed in this study compared to previous *in situ* analyses by Herzog et al. (2008). Uncertainties shown for the $\delta^{41}K$ values in this study are 95 % CI, while uncertainties shown for the Herzog et al. (2008) data are 1SD. As shown, the data from Herzog et al. (2008) show significantly more K isotope variation (both lighter and heavier compositions) compared to the data from this study. V19/29 refers to the single microtektites from cores V19-169 and V29-43.

several microtektites studied by Herzog et al. (2008) show similar $\delta^{41}K$ values both in cores and rims, even for the most highly fractionated microtektites. Core-to-rim K elemental analysis of Transantarctic Mountain microtektites has shown that some samples display internal K_2O variations of up to ~ 0.5 wt% K_2O (Folco et al., 2009), which could result in significant internal $\delta^{41}K$ variation. However, the data in Folco et al. (2009) also show that many microtektites have only limited internal K_2O variation (<0.2 wt%), and the ones that do show large K_2O variations often display the highest K_2O concentrations in both cores and rims, with the distance in-between core and rim showing the lower concentrations. This variation pattern should result in the lowest K isotope fractionation within each microtektite observed at the cores and rims (due to less K depletion), which is not consistent with what is observed when comparing the bulk data from this study and the core and rim data from Herzog et al. (2008). Interestingly, a very similar pattern whereby *in situ* ion microprobe analyses show significantly more fractionation than bulk MC-ICP-MS data for $\delta^{41}K$ has been observed for chondrules (Koefoed et al., 2020). This could indicate that similarities in their environments of formation resulted in significant internal heterogeneities, or, as also discussed in Koefoed et al. (2020) and acknowledged in the *in situ* chondrule $\delta^{41}K$ studies (Alexander and Grossman, 2005; Alexander et al., 2000), instrumental artefacts from the ion microprobe analysis could be the cause.

Even though the *in situ* ion microprobe and bulk MC-ICP-MS analyses show significant differences, there are also some general similarities. Firstly, the majority of microtektites analyzed by Herzog et al. (2008) show both significant depletions in K and large $\delta^{41}K$ variations, much like the MB group in this study. As all microtektites analyzed by Herzog et al. (2008) were sourced from the Indian Ocean, similar to core V19-169 and core V29-43 studied here (which are part of the MB group), this agrees with the observations from this study. Another similarity is that both datasets show $\delta^{41}K$ both above and below the BSE value of –0.43 ± 0.17 ‰ (2SD) (Tuller-Ross et al., 2019), suggesting that Australasian microtektites experienced a complex volatile history, with possibly both evaporation and condensation involved (see Fig. 7A). Nevertheless, in contrast to this study, Herzog et al. (2008) also observed several microtektites with $\delta^{41}K$ values higher than the BSE which were also significantly depleted in K.

4.2. Comparison with other isotope systems

Due to the small size of microtektites resulting in very small quantities of most elements, very few isotopic studies have been applied to them. Yet, a recent study focusing on the Fe isotopic compositions of Australasian microtektites was undertaken whereby significant fractionation was observed (Chernonozhkin et al., 2021). Furthermore, similar to K, Fe shows isotopic compositions both lighter and heavier than the BSE value, with the more extreme fractionation observed for microtektites which travelled over ~3000 km from the proposed source (Chernonozhkin et al., 2021). However, in contrast to the K data from this study, Fe does not show any correlations between concentration and isotope composition. Instead, the microtektites depleted in Fe often show both heavy and light isotopic compositions. Nevertheless, when the Antarctic microtektites are observed on their own, there does appear a slight trend whereby the microtektites depleted in Fe show lighter compositions. Additionally, the most Fe-enriched Antarctic microtektites show $\delta^{56/54}Fe$ values higher than the average UCC composition, similar to what is observed among the MB group microtektites here with K. Yet overall this Fe microtektite data is broadly consistent with the *in situ* K isotope analysis by Herzog et al. (2008). As such, the authors used this Fe isotope data to conclude that microtektite formation involved a convoluted sequence of processes such as condensation, mixing of isotopically distinct reservoirs, and evaporation during atmospheric re-entry (Chernonozhkin et al., 2021).

4.3. Comparison with tektites

In addition to microtektites, tektites (diameter larger than 1 mm) have also been the subject of K isotope analyses. Unlike microtektites, tektites show very limited $\delta^{41}K$ variation, with a total observed range across all tektites from the Australasian, European, and North American tektite strewn fields of ~0.7 ‰ (Herzog et al., 2008; Humayun and Koeberl, 2004; Jiang et al., 2019; Li et al., 2016; Magna et al., 2021). For the Australasian tektites alone, this range is even less, with all high-precision Australasian tektite analysis showing $\delta^{41}K$ values between –0.72 ‰ and –0.26 ‰ (Jiang et al., 2019; Li et al., 2016), which in addition to the limited variation, all cluster around the BSE value of −0.42 ± 0.17 ‰ (Tuller-Ross et al., 2019). As such, the K isotope systematics of tektites provide little insight into their formation, other than that the conditions to produce significant isotopic fractionation of K did not occur. Interestingly, sample 41 from ODP site 1144A, which is by far the largest sample from this study (0.662 mg) and is a fragment (i.e., not a full microtektite), shows a $\delta^{41}K$ composition of –0.51 ± 0.09 ‰ and no depletion in K. It is thus likely that this sample represents a fragment of a larger tektite mass rather than a microtektite.

The isotope compositions of other MVE such as Cu and Zn have also been studied for tektites, yet unlike K, these systems do show significant fractionation, with tektites showing isotopic compositions heavier ($\delta^{65}Cu$ up to 12.5 ‰; $\delta^{66}Zn$ up to 3.7 ‰) than the BSE (Jiang et al., 2019; Moynier et al., 2009; Moynier et al., 2010; Rodovská et al., 2017). As was concluded in these studies, the Cu and Zn isotope compositions, along with significant elemental depletions, strongly support evaporation as the dominant fractionation process. Overall, the Cu, Zn, and K isotope compositions of tektites appear consistent with diffusion-limited evaporation, and "bubble-stripping", which were proposed as possible MVE fractionation mechanisms (Jiang et al., 2019; Melosh and Artemieva, 2004; Moynier et al., 2010; Rodovská et al., 2017). As the Zn and Cu isotopic composition of microtektites cannot be measured currently (their low mass results in total quantities of these elements which are too low), these hypotheses are more difficult to assess for microtektites using the same multi-MVE approach. Nevertheless, as tektites and microtektites display significantly different behaviour for K and Fe, it appears likely that they undergo a different formation process regardless.

4.4. Potassium isotope systematics of Australasian microtektites

The K isotope systematics of Australasian microtektites analyzed here can provide further insights into the formation of microtektites. There appears to be a general trend, especially among the MB microtektite group, whereby lower K concentrations correlate with lighter K isotopic compositions (Fig. 5). This trend is consistent with K partial condensation experiments with preferential condensation of the light isotope over the heavy isotope (Georges et al., 2000). However, the most K-rich MB microtektites show K concentrations well below that of the continental crust and K isotopic compositions (~0.6 ‰) significantly heavier than the BSE (–0.43 ‰), modern seawater (+0.12 ± 0.07 ‰), or any major terrestrial rock type (up to ~ 0.1 ‰) measured to date (Li et al., 2016; Parendo et al., 2017; Tuller-Ross et al., 2019; Wang et al., 2020; Wang and Jacobsen, 2016a; Wang et al., 2021). This makes simple partial condensation from a continental crust-like composition across all Australasian microtektites unlikely, which is not necessarily surprising considering the complexities described by the previous microtektite isotopic studies discussed in sections 4.1.2 and 4.2 (Chernonozhkin et al., 2021; Herzog et al., 2008). Nevertheless, the ODP microtektites show K concentrations close to the UCC composition and K isotopic compositions extending from about the BSE value to ~ 0.6 ‰ lighter. This makes partial condensation appear as the most likely dominant mechanism for the K systematics observed. Nevertheless, as also mentioned in section 4.1.1., mixing of a light-K vapor with a heavy-K liquid based on microtektite surface to mass ratio cannot be ruled out.

Further details surrounding how partial condensation could produce the K isotope systematics observed can be explored by assessing the data in more detail. As shown in Fig. 8, partial condensation of K from a vapor plume starting with a UCC composition, which then evolves over time to become depleted in K and higher in $\delta^{41}K$, could explain the Australasian microtektite K systematics observed here. Under this scenario, the microtektites which condensed K the earliest show only limited isotopic fractionation and K concentrations close to the starting UCC composition. These microtektites were likely within less energetic regions of the plume and did not travel far from the impact site; in this study, they are represented by the ODP microtektites. Following this, some of the now K-depleted vapor was remixed into the remaining plume through turbulence, resulting in the plume on average becoming isotopically heavier and lower in K abundance (the plume composition would have likely been heterogeneous due to incomplete mixing). As the plume continued to expand out and cool, more microtektite K condensation occurred, which along with some mixing within the plume as it expanded, caused the average plume composition to get increasingly depleted in K and isotopically heavy. Thus, microtektites which condensed K later did so from a plume starting composition progressively depleted in K and with a heavier K isotope composition. The MB microtektite group within this study represents these later K condensate microtektites, with their low K concentrations and significant $\delta^{41}K$ fractionation.

This scenario of microtektite K condensation is represented in Fig. 8, with the average vapor composition over time shown by the dashed arrow and an array of Rayleigh fractionation condensation curves from this evolving vapor composition presented as dashed lines. The average vapor composition in this model is constrained by the UCC composition and the isotopically heaviest MB microtektite measured. A fractionation factor (α) of 0.996 was applied for the Rayleigh condensation within this model as it was the best fit for the full dataset. This should, however, be considered an estimate, as the conditions within the vapor plume would have been complex and dynamic which makes establishing a perfect match between samples and calculation essentially impossible.

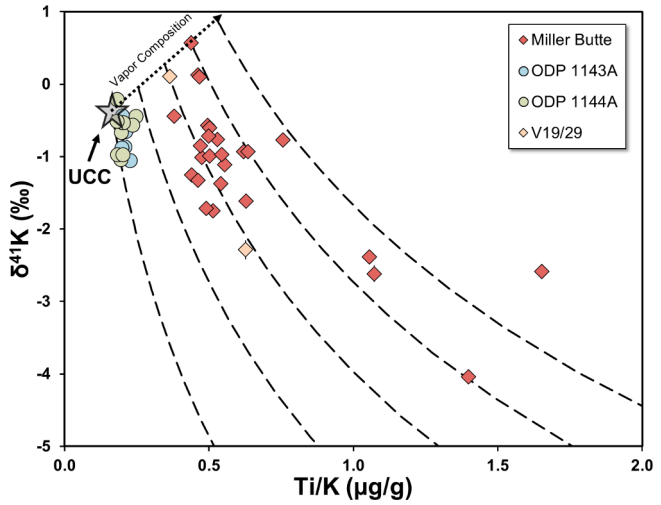

Fig. 8. Plot of K isotope composition vs Ti/K for all microtektites analyzed in this study. Also shown is the proposed condensation model for Australasian microtektites. The dashed lines represent a range of Rayleigh condensation curves over time using an estimated α of 0.996. The dotted line represents the evolving vapor plume composition which is constrained by the UCC (Rudnick and Gao, 2014; Tuller-Ross et al., 2019), shown as a grey star, and the isotopically heaviest microtektite. Uncertainties shown for $\delta^{41}K$ are 95 % CI. As shown, the plume vapor composition evolves over time to become K-depleted and heavier, with the earliest K condensates progressively depleting and fractionating K within the plume. Later condensed microtektites thus condense from a vapor already fractionated and K depleted. V19/29 refers to the single microtektites from cores V19-169 and V29-43.

Nevertheless, K condensation for these Australasian microtektites was certainly inhibited compared to ideal Rayleigh fractionation, as an α of 0.9753 (which represents ideal Rayleigh fractionation in a vacuum for K) is not compatible with either the ODP or MB microtektites. The degree of oversaturation can be expressed as a function of partial pressure (*P*) against saturation pressure (P_{sat}) using the equation $\alpha'-1=(\alpha-1)(1-P_{sat}/P)$, whereby α' represents the effective kinetic isotope fractionation factor and α represents an ideal kinetic isotope fractionation factor (Davis and Richter, 2014). Using this equation, we establish a P_{sat}/P of 0.838, which indicates a degree of oversaturation approaching equilibrium conditions ($P_{sat}/P = 1$), supporting a kinetic fractionation-dominant regime. This calculated P_{sat}/P should be considered an approximation, however, as the α' of 0.996 used for this calculation is an estimate via data best-fit. Additionally, the approximate changes in vapor composition are only constrained by the UCC and heaviest microtektite compositions. Nevertheless, this still allows us to establish that the Australasian microtektite K isotope systematics were most heavily influenced by partial condensation in an evolving vapor plume with predominantly kinetic K isotopic fractionation.

While condensation appears to be the dominant process which influenced K isotope fractionation within the Australasian microtektites studied here, there is some scatter in the data which could indicate that evaporation may have also occurred (e.g., the single ODP microtektite which has a $\delta^{41}K$ value heavier than the UCC). Nevertheless, this is much more strongly evidenced by the previous *in situ* K isotope study by Herzog et al. (2008) which found significant isotopic fractionation but no clear trends, indicating a complex system of evaporation and condensation. It is possible that differences between *in situ* and bulk techniques is why only a strong condensation signature is observed here (see section 4.1.2 for a detailed discussion on this). Alternatively, it could relate to sampling bias within either, or both studies. Sampling variations is a distinct possibility as microtektites are not uniform in their shapes, texture or chemistry, reflecting their different formation histories (Folco et al., 2010b; Glass, 1990; Glass et al., 2004; Glass and Koeberl, 2006). Microtektites can range from teardrop-shaped with vesicles, melted quartz grains (i.e., lechatelierite), pitted and exhibiting schlieren, to spherical clear glass with no strong features (Glass, 1990; Glass and Koeberl, 2006). For this study, the vast majority of microtektites analyzed were spherical, pale yellow and showed limited features (e.g., see Fig. 2). While this is not considered unusual for the Miller Butte microtektites, with ~98 % of Transantarctic Mountain microtektites being pale yellow and spherical (Folco et al., 2009), it is when considering all Australasian microtektites, as a wide range of shapes and textures are observed in Australasian microtektites from other locations (Glass and Koeberl, 2006). At the time of the Herzog et al. (2008) study, the Transantarctic Mountain microtektites had not yet been discovered, so their study consisted of primarily Indian ocean microtektites, of which only two were analyzed here. As such, different primary sampling locations, and thus different microtektites texturally, may have contributed to the differences observed between this study and the study by Herzog et al. (2008). Thus, it is possible that the observations made by Herzog et al. (2008), that some microtektites show evaporation-dominant K isotope fractionation, would have been confirmed in this study too had similar microtektites been analyzed here.

Overall, spherical microtektites with limited features, which are compatible with a condensation-dominant regime, dominate those analyzed in this study. Nevertheless, previous chemical and textual studies indicate that due to vaporization of the impactor, impact condensate spherules should generally contain a significant meteoritic component (Glass et al., 2004; Glass and Simonson, 2013). As most of the microtektites analyzed here show no significant meteoritic component (a few display elevated Cr, Ni, and Co concentrations), this presents a conundrum. It is possible that any meteoritic component is too low to be detected. Yet, it seems unlikely that elements significantly enriched in meteorites compared to the UCC (e.g., Ni) could remain undetectable if any meteoritic component was present in any of the microtektites.

Further investigation of this could be done by conducting a detailed highly siderophile elemental and isotope study, similar to the study by Ackerman et al. (2019) on tektites, but this is outside the scope of this study. Additionally, unlike these siderophile elements, a meteoritic K component could remain undetected, as the UCC has K concentrations over order of magnitude higher than most meteorites. The $\delta^{41}K$ variations observed here are also much larger than what is observed between the UCC and meteorites meaning that any isotopic difference would also be undetectable. Combined, these observations could indicate that the Australasian microtektites studied here were never fully vaporized, beginning as refractory melt ejecta and condensation only occurring for more volatile elements such as K which were vaporized (it is unlikely K was fully vaporized within the whole plume, however, as Jiang et al. (2019) showed Australasian tektites provide no evidence of K condensation or evaporation). Alternatively, if the meteoritic components were distributed unevenly across microtektite condensates, these observations could just support the notion that different Australasian microtektites formed through different processes and from different impact components, and the microtektites studied here represent just a fraction of the overall story. While more data is needed to explore these possibilities further, the latter scenario appears to be more plausible. This is primarily because the microtektites analyzed in this study are predominantly spherical with limited textural features, in contrast to the relic grains, rotational shapes (dumbbells, discs, teardrops), compositional schlieren, and vesicles observed in many Australasian microtektites. Additionally, nearly all the highly isotopically fractionated and K-depleted microtektites analyzed in this study are from a single location (Miller Butte), and are thus unlikely to be representative of all Australasian microtektites. This is further supported by the Herzog et al. (2008) study, which studied a different range of microtektites (i.e., from different locations and possibly with a greater of textures and shapes) and provided evidence for both evaporation and condensation.

4.5. Implications on microtektite formation

4.5.1. Microtektite cooling rates

Recently Nie et al. (2021) developed a model for constraining chondrule cooling rates under a condensation scenario using the total K isotope fractionation and condensed fraction of K. As partial condensation appears to be the dominant process which affected the K systematics within the Australasian microtektites studied here, an adapted version of this model can also be applied here. For a detailed description of the model calculation see Nie et al. (2021). Yet, in brief, during condensation K isotopic fractionation is sensitive to the cooling rate, with a faster cooling rate producing larger fractionation (Richter, 2004). This is largely due to the condensation rate incapable of keeping the system in equilibrium as it cools, producing a supersaturated vapor. In contrast, if the system cools slowly enough, condensation can keep the system in near equilibrium through the cooling process, producing smaller isotopic fractionation. The model developed by Nie et al. (2021) calculated how chondrule cooling rate affected the K isotopic fractionation of the chondrules. This was then presented as total isotopic fractionation against the total condensed fraction of K for different cooling rates, whereby measured chondrule data was then plotted, and a chondrule cooling rate established. For microtektites, several parameters need to be modified compared to those used for chondrules, some of which are not well constrained. Nevertheless, the model can still be successfully applied, allowing us to calculate the estimates for Australasian microtektite cooling rates.

The parameters required to model microtektite cooling rates are peak temperature (T_0), oxygen fugacity (P_{O2}), radius of the melt droplets (r), density of the melt, bulk composition, and fraction of K in melt (as opposed to in the surrounding vapor, assuming each microtektite droplet and its surrounding gas constitute a closed system during cooling) at peak temperature ($f_{K,0}$) (Nie et al., 2021). The peak temperature of Australasian tektites has been calculated to be 2273 K or less, however this was largely based on the lack of K isotopic fractionation in tektites by evaporation (Humayun and Koeberl, 2004). As microtektites show K isotopic fractionation they probably experienced temperatures higher than 2273 K. Nevertheless, this is still the best constraint for microtektite peak temperature and was thus used in the model. For oxygen fugacity, tektites and microtektites are known to be produced under reducing conditions (Giuli et al., 2010; Rossano et al., 1999; Žák et al., 2012), yet the exact conditions are not constrained. Nevertheless, the iron-wustite buffer likely represents conditions close to those experienced during microtektite formation, so this was used for the model. The radius of the melt can be established by the radius of the microtekties, which range from μm ~200 to ~400 μm, with an average of ~300 μm. A density of 2500 kg/m^3 was used for the density of melt here which is identical to what was used by Humayun and Koeberl (2004) for their tektite calculations and within the range used by Chernonozhkin et al. (2021) for their microtektite modeling (2300–2800 kg/m^3). Average UCC was considered as the bulk starting composition (Rudnick and Gao, 2014), as this closely matches microtektite bulk compositions. The fraction of K in melt at peak model temperature was assumed to be 1 %, with 99 % of K in the vapor (i.e., almost completely vaporized), which, when combined with the parameters discussed above, and assuming vapor-melt equilibrium at peak temperature, results in a radius of vapor surrounding the model beads ($\mathcal{R}$) of 0.0488 m (Eq. S16 in Nie et al., 2021). Knowing the $\mathcal{R}$ value, the K isotope fractionation can then be calculated as a function of the condensed K fraction given a certain cooling rate (Eqs. S14 and S15 in Nie et al., 2021).

A model of microtektite cooling rates is shown in Fig. 9, whereby the chondrule cooling model by Nie et al. (2021) has been adapted for microtektites. All microtektites which fit within the parameters are plotted on the model. These plotted points represent the total isotopic fractionations ($(\Delta^{41}K_{condensate} = \delta^{41}K_{condensate} - \delta^{41}K_0)$ and condensed fractions of K (using Ti/K) relative to their starting compositions for each microtektite group. For the ODP group, the UCC represents the

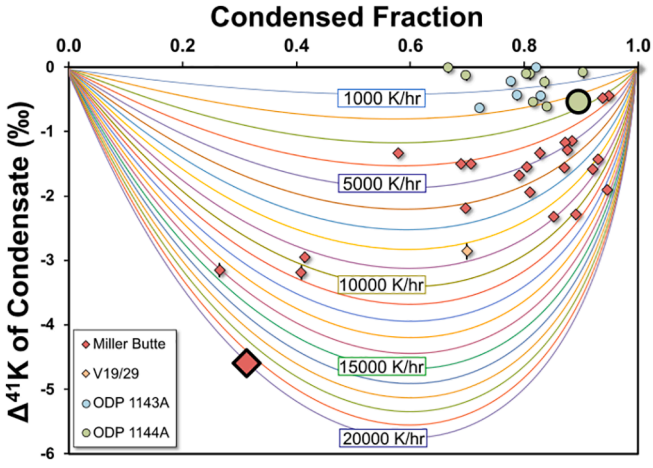

Fig. 9. Plot showing the microtektite condensation cooling rate calculations. Each coloured line represents 1000 K/hour cooling rate change. The enlarged points represent the ODP group microtektite and MB group microtektite with the fastest cooling rate. The plotted points represent the total isotopic fractionations ($\Delta^{41}K_{condensate} = \delta^{41}K_{condensate} - \delta^{41}K_0$) and condensed fractions of K (using Ti/K) relative to their starting compositions for each microtektite group. For the ODP group, the UCC represents the starting K elemental and isotopic composition, while for MB group, the starting K isotope and K concentration is represented by the isotopically heaviest MB microtektite. As shown, maximum cooling rates of 2,600 K/hour and 20,000 K/hour are observed for the ODP and MB group microtektites, respectively. The total range of calculated cooling rates observed is from 0 to 2,600 K/hour for the ODP group, and from 3,200 to 20,000 K/hour for the MB group. V19/29 refers to the single microtektites from cores V19-169 and V29-43.

starting K elemental and isotopic composition, while for MB group, the starting K isotope value and K concentration is represented by the most isotopically heavy MB microtektite as this is our best constraint. When compared with the calculated cooling rate curves (Fig. 9), peak cooling rates of 2600 K/hour and 20,000 K/hour are observed for the ODP and MB group microtektites respectively. For clarity, the microtektite from each group with the fastest cooling rate has been enlarged in Fig. 9. The total range of calculated cooling rates observed is from 0 to 2600 K/hour for the ODP group, and from 3200 to 20,000 K/hour for the MB group. As the OPD and MB group microtektites analyzed here essentially represent endmembers among the Australasian microtektites, it is likely that these also broadly represent the end member cooling rates. Yet, it should be noted that due to the many uncertainties in the parameters of the model, these cooling rates should likely be considered preliminary estimates. Additionally, it is likely the system was much more dynamic than what is presented in this cooling model. This is especially evident for the ODP microtektites, with two calculated as having 0 K/hour cooling rates (due to having no isotopic fractionation relative to the UCC starting composition). Nevertheless, the significant difference between the two microtektite groups does suggest that the close and far travelled microtektites did experience different cooling rates, which is expected since the temperature drops faster further away from the impact plume.

Currently there are no published cooling rates for microtektites. Nevertheless, the cooling rates for Australasian tektites have been previously determined to be 2–23 K/second (7200–82,800 K/hour) by Arndt and Rombach (1976) based on the thermal expansion characteristics. These new cooling rates (2600–20,000 K/hour) for microtektites determined using isotopic fractionation in this study are comparable to those determined on tektites using thermal expansion measurements. In contrast, chondrule cooling rates range from ~10 to 1000 K/hour (Desch et al., 2012; Nie et al., 2021; Radomsky and Hewins, 1990), indicating microtektite cooling rates appear significantly faster. Nevertheless, this is not unexpected as microtektites are primarily glass, while chondrules contain a diverse array of minerals. Additionally, the atmosphere of Earth allows for significantly greater heat transfer compared to the solar nebula.

4.5.2. Formation of Australasian microtektites

As more study is undertaken on microtektites, we are slowly gaining a better understanding of their formation. The K systematics established in this study indicate that condensation from a vapor plume played a significant role in the formation of at least some Australasian microtektites. Additionally, the data clearly show that the vapor plume K composition may have become more depleted and fractionated with time as microtektites condensed K and were removed from the plume. In comparison, previous K and Fe isotopic data from Australasian microtektites indicate a complex series of processes involving condensation and evaporation (Chernonozhkin et al., 2021; Herzog et al., 2008). For Fe, some of this difference could relate to differences in the volatility of K and Fe, with Fe being more refractory than K. This could indicate that elements of different volatilities underwent different processes at different times during the impact event. Additionally, the far travelled Antarctic microtektites, which were analyzed in both studies, were likely travelling fast enough in their descending ballistic trajectories to suffer evaporation by gas drag-related ablation and mass loss during atmosphere re-entry which would further affect their isotopic compositions. For the previous K isotope data, differences in volatility, or chemical affinity for that matter, cannot be a factor. As such, it seems most plausible that sampling differences between the two studies is the dominant factor, with the majority of microtektites studied here being near uniform glass spherules from Miller Butte in Antarctica, while the study by Herzog et al. (2008) primarily analyzed microtektites from Indian Ocean cores which may have had a wider range of textures. When discussing tektites alongside microtektites, the story is further complicated as tektites broadly show no K depletion or K isotope fractionation (Herzog et al., 2008; Humayun and Koeberl, 2004; Jiang et al., 2019; Magna et al., 2021). This indicates that tektites and microtektites could have significantly different formation histories. One possibility is that tektites represent melts from less energetic regions of the impact, while at least some microtektites, originate from material that was either completely or partially vaporized. Nevertheless, significantly more data would be required to understand this further, such as precise K isotope data for microtektites with a wide range of shapes (e.g., dumbbells, teardrops, discs) and textures (e.g., schlieren, lechatelierite, and numerous vesicles), and from a range of different distances from the source.

A detailed physical model describing the formation of both tektites and microtektites is currently still lacking. Reconciling all available data is no easy task, which is made even more difficult due to a complex interplay of multiple processes. Yet, one consistent aspect of many models is the formation of an expanding turbulent plume containing melt, vapor, and supercritical fluid (at the highest pressure–temperature conditions) generated following a large impact (e.g., Collins et al., 2012; Howard, 2011; Johnson and Melosh, 2012; Melosh, 1989; Melosh, 1998). The microtektite formation process discussed here is consistent with such models providing further support for condensation as one significant process affecting the K systematics within Australasian microtektites. Nevertheless, more detailed modelling of large impacts is required in order to better understand the details of complex impact processes. Specifically, more modeling and experiments focused on impact plume dynamics, along the lines of Johnson and Melosh (2012), would be invaluable. Conceivably, the constraints found by this study could be added to the current list of known tektite and microtektite attributes (e.g., reduced chemistry, very low volatile contents, rapid quenching, UCC-like chemical compositions, and the rarity and asymmetry of all tektite strewn fields), in order to help model impacts processes and their relation to tektite and microtektite formation. Overall, the K isotope data from this study, and the isotope data from previous studies, indicate that a complicated interplay between the impacted body, its atmosphere, and the impactor is required to produce the tektite strewn fields observed.

5. Conclusion

In this study we measured the K isotopic and elemental composition of forty-four microtektites from the Australasian strewn field from five different locations ranging from ~1220 km to ~10800 km from the proposed impact site. The isotopic compositions observed range from −4.04 ‰ to 0.57 ‰ $\delta^{41}K$, with the entire range dictated by microtektites from Miller Butte in Antarctica. Additionally, the microtektites found on Miller Butte and the V19/29 locations all show lower K elemental compositions compared to the microtektites found at sites ODP 1144A and 1143A. This information, along with their recovery locations relative to the proposed impact site, resulted in the microtektites analyzed in this study being divided into two groups: 1) the “ODP group” which landed closer to the impact site (~1220–1240 km), shows limited $\delta^{41}K$ variation (–1.06 ‰ to −0.21 ‰) and has high K_2O contents (2.48 wt% to 3.66 wt% K_2O), and 2) the “MB group” which landed further from the impact site (~4100–10800 km), show significant $\delta^{41}K$ variation (−4.04 ‰ to 0.57 ‰) and has low K_2O concentrations (0.49 wt% to 1.45 wt% K_2O). Comparisons with other microtektite elemental data indicate that these two groups likely represent end members of a continuum, rather than two distinct populations.

The overall trend observed among both microtektite groups of lower $\delta^{41}K$ values correlating with lower K elemental concentration is consistent with condensation experiments, indicating that incomplete condensation was likely the dominant process affecting K in the Australasian microtektites studied here. A correlation between microtektite mass and $\delta^{41}K$ was also observed, which could suggest a process such as liquid vapor mixing, yet this observation is also compatible with condensation. The starting K compositions of the ODP group and MB group microtektites appear different, with the ODP group consistent

with a UCC-like K composition, while the MB group indicates a composition lower in K and with a heavier K isotope composition. This evolving starting composition can be explained by the vapor plume K composition changing with time, with the earliest K condensates progressively depleting and fractionating K within the plume, which along with plume mixing through turbulence, altered the starting K compositions for the later formed K condensates. Compared to previous isotopic data on microtektites, which connotes a complicated mixture of condensation, evaporation, and mixing (Chernonozhkin et al., 2021; Herzog et al., 2008), the data here indicate condensation as the dominant process. Nevertheless, evaporation and mixing are also evidenced here by the scatter in the observed data. Using cooling rate calculations based on those conducted on chondrules by Nie et al. (2021), we calculate cooling rates of 2,600 K/hour and 20,000 K/hour for the ODP and MB group microtektites, respectively. Although some of the parameters required for the cooling rate calculations are poorly constrained, these cooling rate estimates of microtektites from the Australasian tektite strewn field are comparable to those determined for Australasian tektites using entirely different approach (i.e., thermal expansion characteristics).

Overall, the exact formation mechanism for the Australasian microtektites remains a conundrum as their compositions, along with the presence of rotational shapes (dumbbells, discs, teardrops), lechatelierite, and vesicles in many microtektites, indicate that they were formed from ejected melt droplets. Furthermore, with rare exceptions, the Australasian microtektites do not contain a detectable meteoritic component as could be expected if they had formed by condensation from the impact plume. On the other hand, the K isotope systematics of the microtektites studied here indicate that condensation from the impact plume played a major role in their formation. Taken together, microtektite formation appears the result of a complicated series of processes whereby both condensation and evaporation played significant roles.

Data availability

Data are available through Mendeley Data at https://doi.org/10.17632/kk98wy4yhn.1.

CRediT authorship contribution statement

Piers Koefoed: Writing – review & editing, Writing – original draft, Supervision, Software, Resources, Project administration, Methodology, Investigation, Formal analysis, Data curation, Conceptualization. **Luigi Folco:** Writing – review & editing, Supervision, Investigation, Conceptualization. **Gianfranco Di Vincenzo:** Writing – review & editing, Investigation, Conceptualization. **Nicole X. Nie:** Writing – review & editing, Software, Investigation. **Billy P. Glass:** Writing – review & editing, Investigation, Conceptualization. **Mason Neuman:** Writing – review & editing, Writing – original draft, Formal analysis. **Kun Wang:** Writing – review & editing, Writing – original draft, Supervision, Investigation, Funding acquisition, Formal analysis, Conceptualization.

Declaration of competing interest

The authors declare that they have no known competing financial interests or personal relationships that could have appeared to influence the work reported in this paper.

Acknowledgments

Piers Koefoed and Kun Wang thank financial support from McDonnell Center for the Space Sciences and NASA (OSIRIS-REx Sample Analysis Participating Scientist Program grant #80NSSC22K1689 and Emerging Worlds Program grant #80NSSC21K0379). Miller Butte microtektites were collected during the 2017 *Programma Nazionale delle Ricerche in Antartide* (PNRA) field campaign. We would also like to thank Tomas Magna for the editorial handling of the manuscript, and Stepan Chernonozhkin, Catherine Macris, and Christian Koeberl for providing insightful reviews and helping to significantly improve the manuscripts quality.

Appendix A. Supplementary material

Supplementary material to this article can be found online at https://doi.org/10.1016/j.gca.2024.06.015.

References

Ackerman, L., Skála, R., Křížová, Š., Žák, K., Magna, T., 2019. The quest for an extraterrestrial component in Muong Nong-type and splash-form Australasian tektites from Laos using highly siderophile elements and Re-Os isotope systematics. Geochim. Cosmochim. Acta 252, 179–189.

Ackerman, L., Žák, K., Skála, R., Rejšek, J., Křížová, Š., Wimpenny, J., Magna, T., 2020. Sr-Nd-Pb isotope systematics of Australasian tektites: implications for the nature and composition of target materials and possible volatile loss of Pb. Geochim. Cosmochim. Acta 276, 135–150.

Alexander, C.M.O.D., Grossman, J.N., 2005. Alkali elemental and potassium isotopic compositions of Semarkona chondrules. Meteorit. Planet. Sci. 40, 541–556.

Alexander, C.M.O.D., Grossman, J.N., Wang, J., Zanda, B., Bourot-Denise, M., Hewins, R. H., 2000. The lack of potassium-isotopic fractionation in Bishunpur chondrules. Meteorit. Planet. Sci. 35, 859–868.

Arndt, J., Rombach, N., 1976. Derivation of the thermal history of tektites and lunar glasses from their thermal expansions characteristics. In: Proceedings of the Seventh Lunar Science Conference, pp. 1123–1141.

Barnes, V.E., 1963. Tektite strewn-fields, in: Tektites. Univ. Chicago Press, pp. 25-50.

Bloom, H., Lodders, K., Chen, H., Zhao, C., Tian, Z., Koefoed, P., Pető, M.K., Jiang, Y., Wang, K., 2020. Potassium isotope compositions of carbonaceous and ordinary chondrites: Implications on the origin of volatile depletion in the early solar system. Geochim. Cosmochim. Acta 277, 111–131.

Burns, C., Glass, B., 1989. Source region for the Australasian tektite strewn field. Meteoritics, vol. 24, p. 257 24, 257.

Chen, H., Meshik, A.P., Pravdivtseva, O.V., Day, J.M.D., Wang, K., 2019a. Potassium isotope fractionation during the high-temperature evaporation determined from the Trinity nuclear test. Chem. Geol. 522, 84–92.

Chen, H., Tian, Z., Tuller-Ross, B., Korotev, R.L., Wang, K., 2019b. High-precision potassium isotopic analysis by MC-ICP-MS: an inter-laboratory comparison and refined K atomic weight. J. Anal. at. Spectrom. 34, 160–171.

Chen, H., Liu, X.-M., Wang, K., 2020. Potassium isotope fractionation during chemical weathering of basalts. Earth Planet. Sci. Lett. 539, 116192.

Chernonozhkin, S.M., González de Vega, C., Artemieva, N., Soens, B., Belza, J., Bolea-Fernandez, E., Van Ginneken, M., Glass, B.P., Folco, L., Genge, M.J., Claeys, P., Vanhaecke, F., Goderis, S., 2021. Isotopic evolution of planetary crusts by hypervelocity impacts evidenced by Fe in microtektites. Nat. Comm. 12, 5646.

Collins, G.S., Melosh, H.J., Osinski, G.R., 2012. The Impact-Cratering Process. Elements 8, 25–30.

Creech, J.B., Moynier, F., Koeberl, C., 2019. Volatile loss under a diffusion-limited regime in tektites: Evidence from tin stable isotopes. Chem. Geol. 528, 119279.

Davis, A.M., Richter, F.M., 2014. 1.10 - Condensation and Evaporation of Solar System Materials. In: Treatise on Geochemistry, second ed. Elsevier, Oxford, pp. 335–360.

Desch, S.J., Morris, M.A., Connolly Jr., H.C., Boss, A.P., 2012. The importance of experiments: Constraints on chondrule formation models. Meteorit. Planet. Sci. 47, 1139–1156.

Di Vincenzo, G., Folco, L., Suttle, M.D., Brase, L., Harvey, R.P., 2021. Multi-collector $^{40}Ar/^{39}Ar$ dating of microtektites from Transantarctic Mountains (Antarctica): A definitive link with the Australasian tektite/microtektite strewn field. Geochim. Cosmochim. Acta 298, 112–130.

Folco, L., Rochette, P., Perchiazzi, N., D'Orazio, M., Laurenzi, M.A., Tiepolo, M., 2008. Microtektites from Victoria Land Transantarctic Mountains. Geology 36, 291–294.

Folco, L., D'Orazio, M., Tiepolo, M., Tonarini, S., Ottolini, L., Perchiazzi, N., Rochette, P., Glass, B.P., 2009. Transantarctic Mountain microtektites: Geochemical affinity with Australasian microtektites. Geochim. Cosmochim. Acta 73, 3694–3722.

Folco, L., Glass, B.P., D'Orazio, M., Rochette, P., 2010a. A common volatilization trend in Transantarctic Mountain and Australasian microtektites: Implications for their formation model and parent crater location. Earth Planet. Sci. Lett. 293, 135–139.

Folco, L., Perchiazzi, N., D'Orazio, M., Frezzotti, M.L., Glass, B.P., Rochette, P., 2010b. Shocked quartz and other mineral inclusions in Australasian microtektites. Geology 38, 211–214.

Folco, L., D'Orazio, M., Gemelli, M., Rochette, P., 2016. Stretching out the Australasian microtektite strewn field in Victoria Land Transantarctic Mountains. Polar Sci. 10, 147–159.

Gentner, W., Kleinmann, B., Wagner, G.A., 1967. New K-Ar and fission track ages of impact glasses and tektites. Earth Planet. Sci. Lett. 2, 83–86.

Georges, P., Libourel, G., Deloule, E., 2000. Experimental constraints on alkali condensation in chondrule formation. Meteorit. Planet. Sci. 35, 1183–1188.

Giuli, G., Eeckhout, S.G., Cicconi, M.R., Koeberl, C., Pratesi, G., Paris, E., Gibson, R.L., Reimold, W.U., 2010. Iron oxidation state and local structure in North American tektites, Large Meteorite Impacts and Planetary Evolution IV. Geol. Soc. Am., p. 0.

Glass, B.P., 1967. Microtektites in Deep-sea Sediments. Nature 214, 372–374.
Glass, B.P., 1978. Australasian microtektites and the stratigraphic age of the australites. GSA Bulletin 89, 1455–1458.
Glass, B.P., 1990. Tektites and microtektites: key facts and inferences. Tectonophysics 171, 393–404.
Glass, B.P., Simonson, B.M., 2013. Distal Impact Ejecta Layers. A Record of Large Impacts in Sedimentary Deposits. Springer, Heidelberg, New York, Dordrecht, London.
Glass, B.P., Huber, H., Koeberl, C., 2004. Geochemistry of Cenozoic microtektites and clinopyroxene-bearing spherules. Geochim. Cosmochim. Acta 68, 3971–4006.
Glass, B.P., Koeberl, C., 2006. Australasian microtektites and associated impact ejecta in the South China Sea and the Middle Pleistocene supereruption of Toba. Meteorit. Planet. Sci. 41, 305–326.
Glass, B.P., Pizzuto, J.E., 1994. Geographic variation in Australasian microtektite concentrations: Implications concerning the location and size of the source crater. J. Geophys. Res. Planets 99, 19075–19081.
Hartung, J.B., 1990. Australasian tektite source crater? Tonle Sap, Cambodia. Meteoritics 25, p. 369 25, 369.
Hartung, J., Koeberl, C., 1994. In search of the Australasian tektite source crater: The Tonle Sap hypothesis. Meteoritics 29, 411–416.
Herzog, G.F., Alexander, C.M.O.D., Berger, E.L., Delaney, J.S., Glass, B.P., 2008. Potassium isotope abundances in Australasian tektites and microtektites. Meteorit. Planet. Sci. 43, 1641–1657.
Howard, K.T., 2011. Volatile enhanced dispersal of high velocity impact melts and the origin of tektites. Proc. Geol. Assoc. 122, 363–382.
Hu, Y., Chen, X.-Y., Xu, Y.-K., Teng, F.-Z., 2018. High-precision analysis of potassium isotopes by HR-MC-ICPMS. Chem. Geol. 493, 100–108.
Humayun, M., Koeberl, C., 2004. Potassium isotopic composition of Australasian tektites. Meteorit. Planet. Sci. 39, 1509–1516.
Jiang, Y., Chen, H., Fegley, B., Lodders, K., Hsu, W., Jacobsen, S.B., Wang, K., 2019. Implications of K, Cu and Zn isotopes for the formation of tektites. Geochim. Cosmochim. Acta 259, 170–187.
Jochum, K.P., Weis, U., Schwager, B., Stoll, B., Wilson, S.A., Haug, G.H., Andreae, M.O., Enzweiler, J., 2016. Reference Values Following ISO Guidelines for Frequently Requested Rock Reference Materials. Geostand. Geoanalytical Res. 40, 333–350.
Johnson, B.C., Melosh, H.J., 2012. Formation of spherules in impact produced vapor plumes. Icarus 217, 416–430.
Jourdan, F., Nomade, S., Wingate, M.T.D., Eroglu, E., Deino, A., 2019. Ultraprecise age and formation temperature of the Australasian tektites constrained by $^{40}Ar/^{39}Ar$ analyses. Meteorit. Planet. Sci. 1–19.
Koeberl, C., 1986. Geochemistry of Tektites and Impact Glasses. Annu. Rev. Earth Planet. Sci. 14, 323–350.
Koeberl, C., 1992. Geochemistry and origin of Muong Nong-type tektites. Geochim. Cosmochim. Acta 56, 1033–1064.
Koeberl, C., Bottomley, R., Glass, B.P., Storzer, D., 1997. Geochemistry and age of Ivory Coast tektites and microtektites. Geochim. Cosmochim. Acta 61, 1745–1772.
Koeberl, C., Glass, B.P., Schulz, T., Wegner, W., Giuli, G., Cicconi, M.R., Trapananti, A., Stabile, P., Cestelli-Guidi, M., Park, J., Herzog, G.F., Caffee, M.W., 2022. Tektite glasses from Belize, Central America: Petrography, geochemistry, and search for a possible meteoritic component. Geochim. Cosmochim. Acta 325, 232–257.
Koefoed, P., Pravdivtseva, O., Chen, H., Gerritzen, C., Thiemens, M.M., Wang, K., 2020. Potassium isotope systematics of the LL4 chondrite Hamlet: Implications for chondrule formation and alteration. Meteorit. Planet. Sci. 55, 1833–1847.
Koefoed, P., Pravdivtseva, O., Ogliore, R., Jiang, Y., Lodders, K., Neuman, M., Wang, K., 2022. The dynamic formation process of the CB Chondrite Gujba. Geochim. Cosmochim. Acta 332, 33–56.
Ku, Y., Jacobsen, S.B., 2020. Potassium isotope anomalies in meteorites inherited from the protosolar molecular cloud. Sci. Adv. 6, eabd0511.
Lee, M.-Y., Wei, K.-Y., 2000. Australasian microtektites in the South China Sea and the West Philippine Sea: Implications for age, size, and location of the impact crater. Meteorit. Planet. Sci. 35, 1151–1155.
Li, W., Beard, B.L., Li, S., 2016. Precise measurement of stable potassium isotope ratios using a single focusing collision cell multi-collector ICP-MS. J. Anal. at. Spectrom. 31, 1023–1029.
Ma, P., Aggrey, K., Tonzola, C., Schnabel, C., de Nicola, P., Herzog, G.F., Wasson, J.T., Glass, B.P., Brown, L., Tera, F., Middleton, R., Klein, J., 2004. Beryllium-10 in Australasian tektites: Constraints on the location of the source crater. Geochim. Cosmochim. Acta 68, 3883–3896.
Magna, T., Deutsch, A., Mezger, K., Skála, R., Seitz, H.M., Mizera, J., Řanda, Z., Adolph, L., 2011. Lithium in tektites and impact glasses: implications for sources, histories and large impacts. Geochim. Cosmochim. Acta 75, 2137–2158.
Magna, T., Jiang, Y., Skála, R., Wang, K., Sossi, P.A., Žák, K., 2021. Potassium elemental and isotope constraints on the formation of tektites and element loss during impacts. Geochim. Cosmochim. Acta 312, 321–342.
Melosh, H.J., 1989. Impact cratering : a geologic process. Oxford University Press, Oxford.
Melosh, H.J., 1998. Impact physics constraints on the origin of tektites. Meteorit. Planet. Sci. 33, A104.
Melosh, H.J., Artemieva, N., 2004. How does Tektite glass lose its water? Lunar and Planetary Science Conference.
Mizera, J., Řanda, Z., Kameník, J., 2016. On a possible parent crater for Australasian tektites: Geochemical, isotopic, geographical and other constraints. Earth Sci. Rev. 154, 123–137.
Moynier, F., Beck, P., Jourdan, F., Yin, Q.-Z., Reimold, U., Koeberl, C., 2009. Isotopic fractionation of zinc in tektites. Earth Planet. Sci. Lett. 277, 482–489.
Moynier, F., Koeberl, C., Beck, P., Jourdan, F., Telouk, P., 2010. Isotopic fractionation of Cu in tektites. Geochim. Cosmochim. Acta 74, 799–807.
Neuman, M., Holzheid, A., Lodders, K., Fegley Jr., B., Jolliff, B.L., Koefoed, P., Chen, H., Wang, K., 2022. High temperature evaporation and isotopic fractionation of K and Cu. Geochim. Cosmochim. Acta 316, 1–20.
Nie, N.X., Chen, X.-Y., Hopp, T., Hu, J.Y., Zhang, Z.J., Teng, F.-Z., Shahar, A., Dauphas, N., 2021. Imprint of chondrule formation on the K and Rb isotopic compositions of carbonaceous meteorites. Sci. Adv. 7, eabl3929.
Nie, N.X., Chen, X.-Y., Zhang, Z.J., Hu, J.Y., Liu, W., Tissot, F.L.H., Teng, F.-Z., Shahar, A., Dauphas, N., 2023. Rubidium and potassium isotopic variations in chondrites and Mars: Accretion signatures and planetary overprints. Geochim. Cosmochim. Acta 344, 207–229.
O'Keefe, J.A., 1976. Tektites and their origin. NASA STI/Recon Technical Report A 77, 14534.
Parendo, C.A., Jacobsen, S.B., Wang, K., 2017. K isotopes as a tracer of seafloor hydrothermal alteration. Proc. Nat. Acad. Sci. U.S.A 114, 1827–1831.
Radomsky, P.M., Hewins, R.H., 1990. Formation conditions of pyroxene-olivine and magnesian olivine chondrules. Geochim. Cosmochim. Acta 54, 3475–3490.
Richter, F.M., 2004. Timescales determining the degree of kinetic isotope fractionation by evaporation and condensation. Geochim. Cosmochim. Acta 68, 4971–4992.
Rochette, P., Braucher, R., Folco, L., Horng, C.S., Aumaître, G., Bourlès, D.L., Keddadouche, K., 2018. ^{10}Be in Australasian microtektites compared to tektites: Size and geographic controls. Geology 46, 803–806.
Rochette, P., Beck, P., Bizzarro, M., Braucher, R., Cornec, J., Debaille, V., Devouard, B., Gattacceca, J., Jourdan, F., Moustard, F., Moynier, F., Nomade, S., Reynard, B., 2021. Impact glasses from Belize represent tektites from the Pleistocene Pantasma impact crater in Nicaragua. Commun. Earth Environ. 2, 94.
Rodovská, Z., Magna, T., Žák, K., Skála, R., Brachaniec, T., Visscher, C., 2016. The fate of moderately volatile elements in impact events—Lithium connection between the Ries sediments and central European tektites. Meteorit. Planet. Sci. 51, 2403–2415.
Rodovská, Z., Magna, T., Žák, K., Kato, C., Savage, P.S., Moynier, F., Skála, R., Ježek, J., 2017. Implications for behavior of volatile elements during impacts—Zinc and copper systematics in sediments from the Ries impact structure and central European tektites. Meteorit. Planet. Sci. 52, 2178–2192.
Rossano, S., Balan, E., Morin, G., Bauer, J.P., Calas, G., Brouder, C., 1999. ^{57}Fe Mössbauer spectroscopy of tektites. Phys. Chem. Miner. 26, 530–538.
Rudnick, R.L., Gao, S., 2014. 4.1 - Composition of the Continental Crust. In: Treatise on Geochemistry, second ed. Elsevier, Oxford, pp. 1–51.
Schwarz, W.H., Trieloff, M., Bollinger, K., Gantert, N., Fernandes, V.A., Meyer, H.-P., Povenmire, H., Jessberger, E.K., Guglielmino, M., Koeberl, C., 2016. Coeval ages of Australasian, Central American and Western Canadian tektites reveal multiple impacts 790ka ago. Geochim. Cosmochim. Acta 178, 307–319.
Sieh, K., Herrin, J., Jicha, B., Angel, D.S., Moore, J.D.P., Banerjee, P., Wiwegwin, W., Sihavong, V., Singer, B., Chualaowanich, T., Charusiri, P., 2020. Australasian impact crater buried under the Bolaven Volcanic field. Southern Laos. Proc. Nat. Acad. Sci. u.s.a. 117, 1346–1352.
Simonson, B.M., Glass, B.P., 2004. SpheruleLayers—Records of Ancient Impacts. Annu. Rev. Earth Planet. Sci. 32, 329–361.
Soens, B., van Ginneken, M., Chernonozhkin, S., Slotte, N., Debaille, V., Vanhaecke, F., Terryn, H., Claeys, P., Goderis, S., 2021. Australasian microtektites across the Antarctic continent: evidence from the Sør Rondane Mountain range (East Antarctica). Geosci. Front. 12, 101153.
Stauffer, P., 1978. Anatomy of the Australasian tektite strewn-field and the probable site of its source crater. In: Proceedings of the 3rd Regional Conference on Geology and Mineral Resources of Southeast Asia, 1978, pp. 285–289.
Tian, Z., Chen, H., Fegley, B., Lodders, K., Barrat, J.-A., Day, J.M.D., Wang, K., 2019. Potassium isotopic compositions of howardite-eucrite-diogenite meteorites. Geochim. Cosmochim. Acta 266, 611–632.
Tian, Z., Magna, T., Day, J.M.D., Mezger, K., Scherer, E.E., Lodders, K., Hin, R.C., Koefoed, P., Bloom, H., Wang, K., 2021. Potassium isotope composition of Mars reveals a mechanism of planetary volatile retention. Proc. Nat. Acad. Sci. u.s.a. 118, e2101155118.
Tuller-Ross, B., Marty, B., Chen, H., Kelley, K.A., Lee, H., Wang, K., 2019. Potassium isotope systematics of oceanic basalts. Geochim. Cosmochim. Acta 259, 144–154.
Van Ginneken, M., Genge, M.J., Harvey, R.P., 2018. A new type of highly-vaporized microtektite from the Transantarctic Mountains. Geochim. Cosmochim. Acta 228, 81–94.
Wang, K., Close, H.G., Tuller-Ross, B., Chen, H., 2020. Global average potassium isotope composition of modern seawater. ACS Earth and Space Chem. 4, 1010–1017.
Wang, K., Jacobsen, S.B., 2016a. An estimate of the Bulk Silicate Earth potassium isotopic composition based on MC-ICPMS measurements of basalts. Geochim. Cosmochim. Acta 178, 223–232.
Wang, K., Jacobsen, S.B., 2016b. Potassium isotopic evidence for a high-energy giant impact origin of the Moon. Nature 538, 487–490.
Wang, K., Li, W., Li, S., Tian, Z., Koefoed, P., Zheng, X.-Y., 2021. Geochemistry and cosmochemistry of potassium stable isotopes. Geochemistry 81, 125786.
Wasson, J.T., 1991. Layered tektites: a multiple impact origin for the Australasian tektites. Earth Planet. Sci. Lett. 102, 95–109.
Wasson, J.T., Ouyang, X., Stovall, W.K., 1990. Uranium volatilization during tektite formation. Meteoritics 25, 419.

Whymark, A., 2021. A review of evidence for a Gulf of Tonkin location for the Australasian tektite source crater. Thai Geoscience J. 2, 1–29.
Yu, Y., Hewins, R.H., Alexander, C.M.O.D., Wang, J., 2003. Experimental study of evaporation and isotopic mass fractionation of potassium in silicate melts. Geochim. Cosmochim. Acta 67, 773–786.
Zähringer, J., Gentner, W., 1963. Radiogenic and atmospheric argon content of tektites. Nature 199, 583.
Žák, K., Skála, R., Řanda, Z., Mizera, J., 2012. A review of volatile compounds in tektites, and carbon content and isotopic composition of moldavite glass. Meteorit. Planet. Sci. 47, 1010–1028.
Zhang, Z.J., Nie, N.X., Mendybaev, R.A., Liu, M.-C., Hu, J.J., Hopp, T., Alp, E.E., Lavina, B., Bullock, E.S., McKeegan, K.D., Dauphas, N., 2021. Loss and isotopic fractionation of alkali elements during diffusion-limited evaporation from molten silicate: theory and experiments. ACS Earth and Space Chem. 5, 755–784.